Spectrochimica Acta Part A: Molecular and Biomolecular Spectroscopy 279 (2022) 121367

Contents lists available at ScienceDirect

Spectrochimica Acta Part A: Molecular and Biomolecular Spectroscopy

journal homepage: www.elsevier.com/locate/saa

VUV–VIS FT spectroscopy of the rare $^{13}C^{18}O$ isotopologue of carbon monoxide: Analysis of the $A^1\Pi(v = 1)$ multiply-perturbed level

Stanisław Ryzner [a], Marzena I. Malicka [b], Alan N. Heays [c], Robert W. Field [d], Nelson de Oliveira [e], Wojciech Szajna [a], Wim Ubachs [f], Rafał Hakalla [a,*]

[a] Materials Spectroscopy Laboratory, Institute of Physics, University of Rzeszów, Pigonia 1 Street, Rzeszów 35-310, Poland
[b] The Faculty of Mathematics and Applied Physics, Rzeszów University of Technology, Powstańców Warszawy 8 Street, Rzeszów 35–959, Poland
[c] J. Heyrovský Institute of Physical Chemistry, Dolejškova 2155/3, Prague 8 182 23, Czech Republic
[d] Department of Chemistry, Massachusetts Institute of Technology, Cambridge, MA02139, USA
[e] Synchrotron SOLEIL, Orme de Merisiers, St. Aubin, BP 48, Gif sur Yvette Cedex, F-91192, France
[f] Department of Physics and Astronomy, and LaserLaB, Vrije Universiteit, De Boelelaan 1081, Amsterdam, 1081 HV, Netherlands

HIGHLIGHTS

- 11 bands of $^{13}C^{18}O$ were obtained by two complementary FT-VIS and FT-VUV methods.
- Deperturbation analysis of $^{13}C^{18}O$ $A^1\Pi(1)$ based on 598 lines was performed.
- The indirect $a^3\Pi(v = 12) \sim A^1\Pi(v = 1)$ interaction were detected and analysed.
- 112 terms of $B^1\Sigma^+(v = 0)$ $J_{max} = 50$ and $C^1\Sigma^+(v = 0)$ $J_{max} = 60$ were calculated.
- 23 parameters for A(1), I(2), d(6), e(3), D(1), a(12) and couplings were determined.

GRAPHICAL ABSTRACT

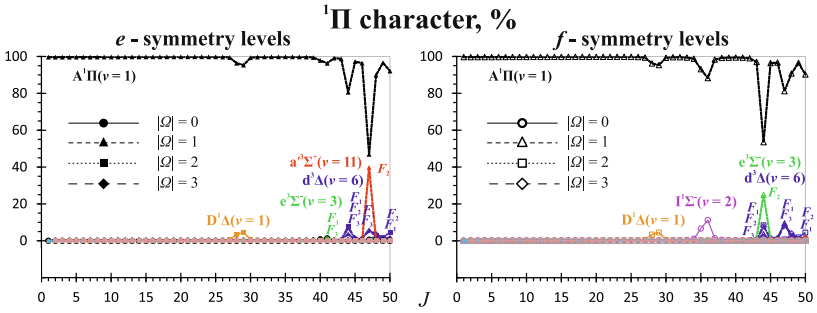

ARTICLE INFO

Article history:
Received 3 March 2022
Received in revised form 5 May 2022
Accepted 6 May 2022
Available online 18 May 2022

Keywords:
High-resolution spectra
VUV-FT absorption and synchrotron spectroscopy
VIS-FT emission spectroscopy
CO
Carbon monoxide
$^{13}C^{18}O$ $A^1\Pi(v = 1)$ multiply-perturbed level
Deperturbation analysis
Spin-orbit and spin-electronic and rotation-electronic (L-uncoupling) and spin-spin interactions

ABSTRACT

Ro-vibronic spectra of the $^{13}C^{18}O$ carbon monoxide isotopologue were obtained with *(i)* emission spectroscopy in the visible region using a Bruker IFS 125HR spectrometer (University of Rzeszów) and *(ii)* vacuum-ultraviolet absorption spectroscopy using the wave-front-division spectrometer on the DESIRS beamline of the SOLEIL synchrotron. A deperturbation analysis of the $^{13}C^{18}O$ $A^1\Pi(v = 1)$ level was conducted from 598 observed transitions from the $B^1\Sigma^+ - A^1\Pi(0, 1)$, $C^1\Sigma^+ - A^1\Pi(0, 1)$, $A^1\Pi - X^1\Sigma^+(1, 0)$, $B^1\Sigma^+ - X^1\Sigma^+(0, 0)$, $C^1\Sigma^+ - X^1\Sigma^+(0, 0)$, $I^1\Sigma^- - X^1\Sigma^+(2, 0)$ bands and five further nominally forbidden bands. An effective Hamiltonian and *term-value fitting analysis* was implemented. Consequently, 135 parameters were floated: 23 molecular parameters, including molecular constants for $A^1\Pi(v = 1)$, $I^1\Sigma^-(v = 2)$, $d^3\Delta(v = 6)$, $e^3\Sigma^-(v = 3)$ and $D^1\Delta(v = 1)$; rotation-electronic (***L***-uncoupling) mixing of $A^1\Pi(v = 1) \sim [D^1\Delta(v = 1), I^1\Sigma^-(v = 1), I^1\Sigma^-(v = 2)]$ and spin–orbit interaction parameters for $A^1\Pi(v = 1) \sim [d^3\Delta(v = 6), e^3\Sigma^-(v = 3), a'^3\Sigma^+(v = 11)]$; the spin–orbit/spin-electronic/***L***-uncoupling $a^3\Pi(v = 12) \sim d^3\Delta(v = 5)$ and spin–orbit $a^3\Pi(v = 12) \sim [D^1\Delta(v = 1), I^1\Sigma^-(v = 2)]$ perturbation parameters; as well as 112 ro-vibronic term values of $B^1\Sigma^+(v = 0)$ up to $J = 50$ and $C^1\Sigma^+(v = 0)$ up to $J = 60$. The significant, indirect $a^3\Pi(v = 12) \sim [e^3\Sigma^-(v = 2, 3), d^3\Delta(v = 5, 6)] \sim A^1\Pi(v = 1)$ spin–orbit/spin-electronic/***L***-uncoupling interaction and $a^3\Pi(v = 12) \sim [I^1\Sigma^-(v = 2), D^1\Delta(v = 1)] \sim A^1\Pi(v = 1)$ spin–orbit/***L***-uncoupling interaction were detected and analysed. Thus, this study, using modern experimental methods and deperturbation analysis, leads to a much improved description in terms of molecular constants and interaction parameters, compared to previous studies of the $A^1\Pi(v = 1)$ energy region in the $^{13}C^{18}O$ isotopologue. This research is

* Corresponding author.
E-mail address: rhakalla@ur.edu.pl (R. Hakalla).

https://doi.org/10.1016/j.saa.2022.121367
1386-1425/© 2022 The Author(s). Published by Elsevier B.V.
This is an open access article under the CC BY license (http://creativecommons.org/licenses/by/4.0/).

a continuation of the studies on the $A^1\Pi$ state and its numerous perturbers in the CO isotopologues made by our team.

© 2022 The Author(s). Published by Elsevier B.V. This is an open access article under the CC BY license (http://creativecommons.org/licenses/by/4.0/).

1. Introduction

Carbon monoxide is the second most abundant molecular species in the Universe. CO is used as a physicochemical benchmark in many astronomical environments, such as: interstellar clouds [1–3], circumstellar discs, as well as planetary [4,5] and exoplanetary atmospheres [6,7]. It has become crucial to obtain precise values of the molecular parameters of various CO isotopologues, as they facilitate study of the chemical evolution of low-mass star formation and solar nebula and protoplanetary discs [8–10] as well as planetary nebulae [11]. By determining the CO abundance, it is possible to map the density of matter in the universe and to determine the percentage of molecular hydrogen in interstellar clouds, for which CO and its isotopologues act as a tracer [12–14]. Carbon monoxide is also a typical product of incomplete combustion, and therefore a good knowledge of its properties, including its spectroscopy, is important in ecology and industry [15]. From a pure-spectroscopy perspective the CO molecule is a benchmark species for the investigation of perturbations in the spectroscopy of diatomic molecules. In particular the energy level structure of the first excited singlet state of CO, i.e. $A^1\Pi$, exhibits a wealth of perturbations in all isotopologues, including $^{13}C^{18}O$.

The complex energy structure of the $A^1\Pi$ state results from extensive multi-state interactions with the $a'^3\Sigma^+$, $e^3\Sigma^-$, $d^3\Delta$, $I^1\Sigma^-$ and $D^1\Delta$ states [16,17] and indirect perturbation by the $a^3\Pi$ state [17]. The first deperturbation analyses of the $A^1\Pi$ state were made by Field [18] and Field et al. [19] for the main $^{12}C^{16}O$ isotopologue on the basis of experimental frequencies of transitions in the $A^1\Pi$ (v = 0–23) - $X^1\Sigma^+(v = 0)$ bands with accuracies of about 0.1 cm^{-1}. Our previous reanalysis of the $A^1\Pi$ level in $^{12}C^{16}O$ was based on data from two experiments: two-photon Doppler-free laser spectroscopy with an accuracy of ca. 0.002 cm^{-1} and Fourier-transform (FT) vacuum ultraviolet (VUV) spectroscopy associated with synchrotron radiation with an accuracy up to 0.01 cm^{-1} [20,21]. Deperturbation analyses of $A^1\Pi$ levels of the less-abundant isotopologues were made by us in: *(i)* $^{13}C^{16}O$ [22] and $^{12}C^{18}O$ [23] using three complementary techniques, VIS-FT, VUV-FT and two-photon Doppler-free spectroscopies with accuracies up to 0.005, 0.02, and 0.003 cm^{-1}, respectively; *(ii)* $^{12}C^{17}O$ [24] and $^{13}C^{17}O$ [25] by means of two Fourier-transform methods (VUV-FT and VIS-FT) with accuracies of about 0.01 and 0.003 cm^{-1}, respectively. Our latest deperturbation analyses of the $A^1\Pi$ level were performed by Malicka et al. [26,35] in $^{12}C^{18}O$, by VIS-FT and VUV-FT spectroscopy with accuracies of ca. 0.005 cm^{-1} and 0.01 cm^{-1}, respectively.

Two deperturbation analyses have been made for the $^{13}C^{18}O$ isotopologue so far. The first, by Haridass et al. [27] studied the v = 1 vibrational level after recording the $A^1\Pi$ - $X^1\Sigma^+$ system using the 10.6 m vacuum spectrometer installed at the National Research Council of Canada laboratory. The absolute frequency accuracy was about 0.1 cm^{-1}. A second analysis was performed by Hakalla et al. [17] for the v = 0 level and provided the first example of observations and analysis of the indirect $a^3\Pi \sim A^1\Pi$ interaction in the carbon monoxide molecule. The work was carried out using three complementary spectroscopic methods: *(i)* emission VIS-FT spectroscopy with the accuracy of ca. 0.005 cm^{-1} by means of a Bruker IFS 125HR UV–VIS spectrometer (University of Rzeszów); *(ii)* absorption VUV-FT spectroscopy (accuracy about 0.02 cm^{-1}) using VUV-FT spectrometer (SOLEIL synchrotron); *(iii)* two-photon Doppler-free VUV laser spectroscopy with accuracy up to 0.003 cm^{-1} by means of a narrowband laser source consisting of a pulsed-dye-amplifier (PDA) injection seeded by the continuous-wave output of a ring-dye laser (LaserLab, Vrije Universiteit, Amsterdam) [28].

Spectra concerning the $A^1\Pi$ (v = 1) level in $^{13}C^{18}O$ are recorded previously by Malak et al. [29], Prasad et al. [30,31], Kępa [32,33], and Lemaire et al. [34] who variously study the B - A, C - A, E - A, and A - X systems. However, no deperturbation analysis was carried out in these works and this experimental data is for $A^1\Pi$ (v = 1) levels with $J \leq 40$, which we extend to J = 45 in this work. Additionally, a significantly greater number of extra lines attributable to intersystem transitions are observed in the current work than previously. Most importantly, the precision of $A^1\Pi(v = 1)$ term values determined in this work is a 5 to 10 times improvement.

Here, we extend our previous analysis [17] of the first vibrational level $A^1\Pi(v = 0)$ in the $^{13}C^{18}O$ isotopologue and unravel the energy structure of the v = 1 level using modern experimental methods, and significantly extended the deperturbation analysis of this level compared with Ref. [27]. This research is a continuation of the studies on the $A^1\Pi$ state and its numerous perturbers in the CO isotopologues made by our team [17,20,22–26,35]. Our goal is to quantify all perturbations affecting the $A^1\Pi$ state of CO in all isotopologues and, ultimately, in a mass-independent form.

2. Experimental details

2.1. VIS-FT emission spectroscopy

An air-cooled hollow-cathode lamp was used to produce $^{13}C^{18}O$ molecules. In order to deposit ^{13}C nanoparticles inside the hollow cathode, the lamp was filled with a mixture of helium (as a carrier gas) and $^{13}C_2D_2$ (Cambridge Isotopes, 99.98% of ^{13}C) gases under a pressure of about 13 mbar. An electrical voltage was applied to the electrodes for 150 h with a current of 100 mA DC flowing through the gas mixture. A similar process was used in Refs. [36–39]. The lamp was then pumped out and filled with a portion of isotopically-enriched oxygen $^{18}O_2$ (Sigma Aldrich, $^{18}O_2$ 98.1%) at a pressure of about 4 mbar. After the cathode effect was initiated, $^{13}C^{18}O$ molecules began to form in the tube. During data acquisition, the spectrum source was operating at 880 V and 80 mA DC. The temperature of the intra-cathode molecules was about (1050 ± 50) K, which allowed for an observable population of rotational levels up to J = 45 and 29 of the $B^1\Sigma^+$ and $C^1\Sigma^+$ states, respectively.

The spectrum was recorded under vacuum conditions using a Bruker (IFS 125HR) FT spectrometer installed at the University of Rzeszów. The instrumental resolution was set to 0.018 cm^{-1} during the acquisition of 128 scans. A calibration of the frequency axis was achieved with a 0.004 cm^{-1} (1σ) uncertainty by reference to the He-Ne line (633 nm) generated by a stabilized laser designed to measure the position of the movable mirror in the interferometer.

Molecular line positions were determined by fitting Voigt profiles to the measured contours using commercial Bruker software – OPUS 7.5 [40]. In order to achieve higher accuracy, each single spectral contour was analysed independently. The absolute accuracy was computed by Gaussian error propagation including the calibration uncertainty and uncertainty of line profile fitting, which

is approximated by means of the empirical formula after Brault [41]:

$$\delta\sigma = \frac{k}{\sqrt{N_w}} \frac{FWHM}{SNR} \quad (1)$$

where k is a constant of order unity that depends on the algorithm and the line shape; the value of k for a Voigt profile is between 0.75 (a common choice) and 1 (conservative), N_w is the number of statistically-independent points within one line width, i.e. the number of points above the half-maximum intensity of the line contour (N) divided by the zero-filling factor (ZFF) employed in the inverse Fourier-transform, $FWHM$ is the full width at half maximum of the line profile, and SNR is the signal-to-noise ratio.

The estimated uncertainties for the line-positions are subjectively doubled for blended lines because of correlation effects not included in the Brault formula. As a result, the wavenumbers of $B^1\Sigma^+$ - $A^1\Pi(0, 1)$ transitions were obtained with absolute accuracies of about 0.008 and 0.012 cm^{-1}, respectively, for isolated and blended lines. The accuracy of $C^1\Sigma^+$ - $A^1\Pi(0, 1)$ line frequencies is about 0.04 cm^{-1}. Fig. 1 and Fig. 2 show experimental spectra for the $^{13}C^{18}O$ $B^1\Sigma^+$ - $A^1\Pi(0, 1)$ and $C^1\Sigma^+$ - $A^1\Pi(0, 1)$ bands, respectively, along with simulations generated with the PGOPHER program [42,43]. Overlapping bands of $^{12}C^{18}O$ $B^1\Sigma^+$ - $A^1\Pi(0, 1)$ [26], $^{13}C^{16}O$ $B^1\Sigma^+$ - $A^1\Pi(0, 1)$ [38], $^{12}C^{18}O$ $C^1\Sigma^+$ - $A^1\Pi(0, 4)$ [44], and $^{12}C^{18}O$ $C^1\Sigma^+$ - $A^1\Pi(0, 1)$ [26] bands are taken into consideration in the analysis. Measured line-centre wavenumbers are collected in Table 1 for $B^1\Sigma^+$ - $A^1\Pi(0, 1)$ and in Table 2 for $C^1\Sigma^+$ - $A^1\Pi(0, 1)$. In the recorded spectra there appear five extra lines from forbidden bands, resulting from the interaction of the $A^1\Pi(v = 1)$ level with perturbing levels. The extra lines are listed in Table 3.

2.2. VUV-FT absorption, synchrotron spectroscopy

Photoabsorption spectra including $A^1\Pi$ – $X^1\Sigma^+(1, 0)$ and some nearby forbidden transitions were recorded by VUV Fourier-transform spectroscopy on the DESIRS beamline at the SOLEIL synchrotron. Details of this all-reflection windowless spectrometer and synchrotron radiation source are given elsewhere [45,46]. For this analysis, three room-temperature spectra were recorded with increasing column density of a purified $^{13}C^{18}O$ sample. The frequencies of all observed lines were deduced by least-squares optimising a simulation of the experimental spectra, as was done in our previous work e.g., [26,35].

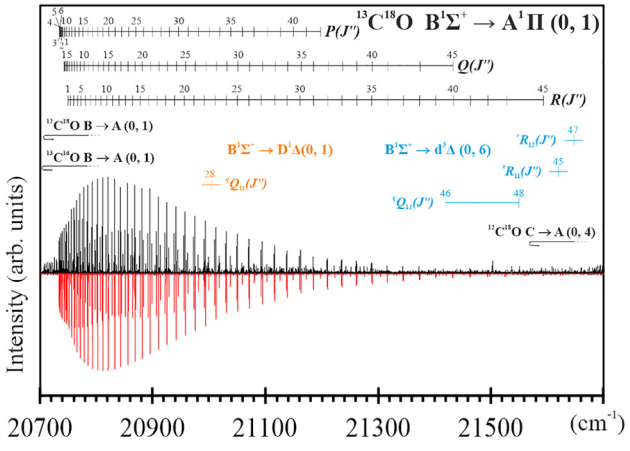

Fig. 1. Experimental $^{13}C^{18}O$ $B^1\Sigma^+$ - $A^1\Pi(0, 1)$ spectrum obtained by means of VIS-FT spectroscopy technique (upper, black trace) as well as simulated after deperturbation one (lower, red trace) using PGOPHER code [43]. The $^{12}C^{18}O$ $B^1\Sigma^+$ - $A^1\Pi(0, 1)$, $^{13}C^{16}O$ $B^1\Sigma^+$ - $A^1\Pi(0, 1)$ and $^{12}C^{18}O$ $C^1\Sigma^+$ - $A^1\Pi(0, 4)$ bands, coexisting in the spectrum, have been taken into account in the analysis as the contaminations of the considered band.

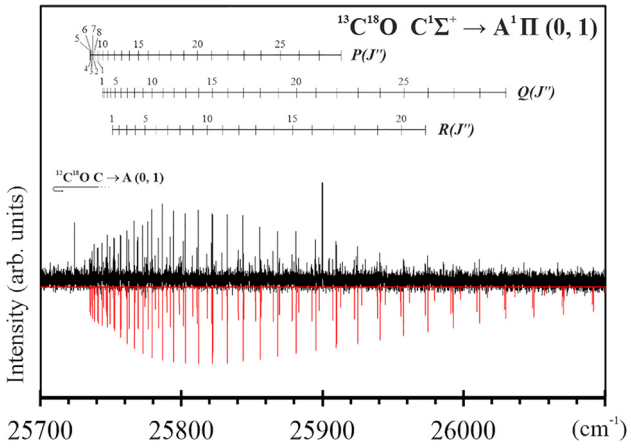

Fig. 2. Experimental $^{13}C^{18}O$ $C^1\Sigma^+$ - $A^1\Pi(0, 1)$ spectrum obtained by means of VIS-FT spectroscopy technique (upper, black trace) as well as simulated after deperturbation one (lower, red trace) using PGOPHER code [43]. The $^{12}C^{18}O$ $C^1\Sigma^+$ - $A^1\Pi(0, 1)$ band, coexisting in the spectrum, has been taken into account in the analysis as the contaminations of the considered band.

Fig. 3 shows the measured spectra and assigned $^{13}C^{18}O$ $A^1\Pi$ – $X^1\Sigma^+(1, 0)$ lines. Many further lines are evident in the highest column density spectrum arising from contamination by other CO isotopologues and forbidden transitions of $^{13}C^{18}O$. The assigned of the latter ones are listed in Table 4, Table 5 and Table 6. An absolute frequency calibration of these spectra was made with reference to the known frequencies of $A^1\Pi$ – $X^1\Sigma^+(0, 0)$ transitions [17], which appear within the synchrotron radiation band pass used to measure $A^1\Pi$ – $X^1\Sigma^+(1, 0)$. The systematic calibration uncertainty of measured frequencies and resulting energy levels is 0.01 cm^{-1}, and is combined in Table 4 and Table 5 with random fitting errors estimated for each line. Line frequencies of the $^{13}C^{18}O$ $B^1\Sigma^+$ – $X^1\Sigma^+(0, 0)$ and $C^1\Sigma^+$ – $X^1\Sigma^+(0, 0)$ bands were measured from SOLEIL spectra by Hakalla et al. (Ref. [17], Table 9) and in this work, respectively. A list of the $C^1\Sigma^+$ - $X^1\Sigma^+(0, 0)$ wavenumbers is provided in Table 7.

3. Deperturbation analysis

The states perturbing $A^1\Pi(v = 1)$ in $^{13}C^{18}O$ are: *(i)* $a'^3\Sigma^+(v = 10, 11)$, $e^3\Sigma^-(v = 2, 3)$, $d^3\Delta(v = 5, 6)$ triplet levels, which are homogeneously coupled with $A^1\Pi(v = 1)$ due to spin–orbit interactions (parameterized here by η); *(ii)* $I^1\Sigma^-(v = 1, 2)$ and $D^1\Delta(v = 1)$ singlet levels heterogeneously coupled with $A^1\Pi(v = 1)$ via rotation-electronic ($\boldsymbol{L}$ – uncoupling) interactions (parameterized by ξ) [16,19,47,48]; *(iii)* $a^3\Pi(v = 12)$, which is coupled to $A^1\Pi(v = 1)$ by means of a direct but negligibly weak spin–orbit interaction as well as indirect and measurable spin–orbit, spin-electronic, and rotation-electronic ($\boldsymbol{L}$-uncoupling) interactions [17,35].

A quantum–mechanical model of $A^1\Pi(v = 1)$ and its perturbers was built using a development version of the PGOPHER program [43] as well as a diagram of the energy neighbourhood of $A^1\Pi$ ($v = 1$) presented in Fig. 4. The properties of $A^1\Pi(v = 1)$ and its perturbers are expressed in the model as matrix elements in an effective Hamiltonian, whilst $B^1\Sigma^+(v = 0)$ and $C^1\Sigma^+(v = 0)$ states were represented by term values, in a *term-value fitting approach* [49–52]. This method eliminates the influence of so-far-unidentified perturbations affecting the $B^1\Sigma^+(v = 0)$ and $C^1\Sigma^+(v = 0)$ levels (Ref. [17]) when deperturbing $A^1\Pi(v = 1)$. The model, defined in this way, was iteratively fitted to 598 experimental wavenumbers derived from 11 bands of $^{13}C^{18}O$, i.e.: $B^1\Sigma^+$ - $A^1\Pi(0, 1)$, $C^1\Sigma^+$ - $A^1\Pi$

Table 1
Wavenumbers of the VIS-FT $B^1\Sigma^+$ - $A^1\Pi(0, 1)$ emission band in $^{13}C^{18}O$.[a,b]

J″	R(J″)	o–c	Q(J″)	o–c	P(J″)	o–c
1	20,749.04(2)	–0.01	20,741.961(9)[b]	–0.001	20,738.42(2)[b]	0.01
2	20,753.915(8)	0.002	20,743.297(5)	0.001	20,736.218(6)	0.003
3	20,759.451(6)	–0.001	20,745.295(5)	–0.001	20,734.681(5)	0.003
4	20,765.653(5)	–0.004	20,747.961(5)	0.001	20,733.807(5)	0.002
5	20,772.528(5)	0.002	20,751.297(5)	0.003	20,733.601(6)[b]	0.002
6	20,780.063(5)	0.001	20,755.292(5)	–0.001	20,734.062(6)[b]	0.001
7	20,788.264(6)[b]	0.001	20,759.957(5)	–0.001	20,735.189(5)	–0.001
8	20,797.130(6)[b]	0.001	20,765.288(5)	–0.001	20,736.986(5)	0.001
9	20,806.661(5)[b]	0.002	20,771.285(5)[b]	–0.001	20,739.448(5)	0.001
10	20,816.855(5)	0.001	20,777.948(5)[b]	–0.001	20,742.577(5)	0.001
11	20,827.717(5)	0.001	20,785.277(5)	–0.001	20,746.373(5)[b]	0.001
12	20,839.239(5)[b]	0.001	20,793.273(5)	–0.002	20,750.837(5)	0.001
13	20,851.427(5)	0.002	20,801.932(5)	–0.001	20,755.971(5)[b]	0.002
14	20,864.279(5)[b]	0.003	20,811.258(5)	–0.002	20,761.768(5)	0.001
15	20,877.793(5)	0.001	20,821.251(5)[b]	–0.002	20,768.235(5)	0.001
16	20,891.932(5)	0.002	20,831.909(5)	–0.001	20,775.369(5)[b]	–0.001
17	20,906.815(5)	0.002	20,843.193(5)[b]	–0.002	20,783.172(5)[b]	0.001
18	20,922.332(5)	0.002	20,855.226(5)	–0.002	20,791.604(5)	0.001
19	20,938.503(5)	0.001	20,867.893(5)	–0.002	20,800.785(5)	0.002
20	20,955.341(5)	0.002	20,881.219(5)[b]	–0.002	20,810.604(5)	0.001
21	20,972.846(5)[b]	0.003	20,895.215(5)[b]	–0.002	20,821.087(5)[b]	0.003
22	20,991.014(5)	0.002	20,909.881(5)	–0.002	20,832.240(5)	0.002
23	21,009.849(5)	0.002	20,925.217(5)[b]	–0.002	20,844.066(5)	0.001
24	21,029.351(5)	0.003	20,941.224(5)[b]	–0.002	20,856.569(5)	0.002
25	21,049.527(5)	0.001	20,957.903(5)	–0.002	20,869.745(5)	0.001
26	21,070.378(5)	–0.002	20,975.269(5)	–0.002	20,883.602(5)	–0.001
27	21,091.921(5)	–0.002	20,993.334(5)	–0.004	20,898.169(5)	0.002
28	21,114.323(5)	0.001	21,012.259(5)	–0.002	20,913.599(5)	0.005
29	21,136.363(5)	0.001	21,030.831(5)	0.003	20,928.672(5)	0.005
30	21,160.132(5)	0.003	21,051.138(5)[b]	0.001	20,945.483(5)	0.001
31	21,184.340(6)	–0.004	21,071.902(5)	0.001	20,962.748(5)	0.001
32	21,209.210(6)	–0.001	21,093.325(6)[b]	0.002	20,980.654(7)[b]	–0.001
33	21,234.727(6)	0.001	21,115.457(5)	0.003	20,999.236(6)	0.004
34	21,260.93(1)[b]	0.01	21,138.336(5)	0.002	21,018.499(8)[b]	0.001
35	21,287.76(2)[b]	0.01	21,162.398(7)[b]	0.005	21,038.432(8)[b]	–0.002
36	21,315.29(2)[b]	0.01	21,183.971(8)[b]	–0.004	21,059.069(7)	–0.002
37	21,343.48(2)[b]	–0.01	21,209.664(6)	0.004	21,080.35(2)[b]	0.01
38	21,372.36(2)[b]	–0.03	21,235.294(6)	0.008	21,102.35(2)[b]	0.01
39	21,401.93(3)[b]	–0.01	21,261.54(1)[b]	0.04	21,125.06(1)	–0.02
40	21,432.34(7)[bw]	0.01	21,288.30(2)[b]	–0.02	21,148.57(2)[b]	–0.03
41	21,462.56(3)[w]	0.01	21,315.88(4)[bw]	–0.01	21,171.94(2)[b]	–0.02
42	21,494.52(4)[bw]	0.04	–	–	21,197.05(3)[w]	0.01
43	21,527.00(3)[bw]	0.04	21,373.40(3)[w]	–0.01	–	–
44	–	–	–	–	–	–
45	21,593.12(5)[w]	–0.02	21,431.87(3)[w]	0.01	–	–

[a] In cm^{-1}. *o–c* mean the observed minus calculated values. The instrumental resolution was 0.018 cm^{-1}. The estimated absolute calibration uncertainty was 0.004 cm^{-1}. The uncertainties in parentheses indicate 1σ standard deviations being combinations of fitting and calibration errors. The absolute accuracy of the line frequency measurements was estimated to fall between 0.008 and 0.012 cm^{-1}, depending on the line intensity and blending.
[b] Lines marked with *b* and/or *w* are blended and/or weak.

(0, 1), $A^1\Pi$ - $X^1\Sigma^+(1, 0)$, $B^1\Sigma^+$ - $X^1\Sigma^+(0, 0)$, $C^1\Sigma^+$ - $X^1\Sigma^+(0, 0)$, $B^1\Sigma^+$ - $d^3\Delta(0, 6)$, $B^1\Sigma^+$ - $D^1\Delta(0, 1)$, $d^3\Delta$ - $X^1\Sigma^+(6, 0)$, $e^3\Sigma^-$ - $X^1\Sigma^+(3, 0)$, $I^1\Sigma^-$ - $X^1\Sigma^+(2, 0)$ and $D^1\Delta$ - $X^1\Sigma^+(1, 0)$, until a satisfactory agreement was achieved. Full details of this methodology are presented in our previous works [17,24–26,35,53] and the Hamiltonian is described by Western [42]. The output (*.log) file of PGOPHER program, containing the explicit-formulated effective Hamiltonian and matrix elements, is available in the supplementary material. Definitions of the η and ξ interaction parameters are precisely described in Refs. [17,24,25] and their relations to the symbols α and β previously used in the literature are as follows:

$$\eta_{A\sim e,d,a'} = -\alpha_{A\sim e,d,a'} \times \sqrt{3} \quad (2)$$

$$\xi_{A\sim I} = -\beta_{A\sim I} \times \sqrt{2} \quad (3)$$

$$\xi_{A\sim D} = \beta_{A\sim D} \quad (4)$$

$$\eta_{a\sim I,D} = -\alpha_{a\sim I,D} \times \sqrt{3} \quad (5)$$

$$\eta_{a\sim e,d,a'} = -\left(\alpha_{a\sim e,d,a'} + \beta_{a\sim e,d,a'}\right) \times 2\sqrt{3} \quad (6)$$

$$\xi_{a\sim e,d,a'} = \beta_{a\sim e,d,a'} \quad (7)$$

Values of the molecular parameters used in an initial model were taken from Refs. [18–21,47,54,55] and isotopically scaled while correcting for our use of the total angular momentum operator ($\widehat{\boldsymbol{N}}$) that differs from the operator for angular momentum of the nuclear framework ($\widehat{\boldsymbol{R}}$) used in the cited works (see Malicka et al. 2020 [26]). Molecular constants for the $^{13}C^{18}O$ $X^1\Sigma^+(v = 0)$ ground state were taken from Ref. [56] and kept fixed in all fits. At a preliminary stage of the analysis, the data from Refs. [17–19,24,47,57] were used as the basis for the calculation of the interaction parameters. In cases where these interactions are significant but correlated with other less well-known parameters (see Table 8 for details), their values were kept fixed in the fits. To avoid overfitting our multi-parameter model, the correlation matrix was constantly monitored throughout the analysis for significant statistical relationships between variables. The root-mean-square error

Table 2
Wavenumbers of the VIS-FT $C^1\Sigma^+$ - $A^1\Pi(0, 1)$ emission band in $^{13}C^{18}O$.[a,b]

J″	R(J″)	o–c	Q(J″)	o–c	P(J″)	o–c
1	25,750.46(7)[bw]	−0.03	25,743.44(5)[bw]	0.04	25,739.87(6)[bw]	−0.02
2	25,755.31(3)[bw]	−0.02	25,744.75(4)[bw]	0.02	25,737.68(3)[w]	0.02
3	25,760.82(4)[bw]	−0.02	25,746.71(4)[bw]	−0.01	25,736.12(3)[bw]	0.02
4	25,767.04(6)[bw]	0.03	25,749.34(3)[b]	−0.01	25,735.25(5)[bw]	0.03
5	25,773.83(3)[bw]	−0.02	25,752.67(3)[b]	0.02	25,735.00(3)[bw]	0.02
6	25,781.35(3)[bw]	0.02	25,756.61(2)[b]	0.01	25,735.42(4)[bw]	0.01
7	25,789.50(3)[bw]	0.02	25,761.23(2)[b]	0.01	25,736.52(3)[b]	0.02
8	25,798.29(4)[bw]	0.01	25,766.53(3)[b]	0.03	25,738.25(3)[b]	−0.01
9	25,807.78(4)[bw]	0.04	25,772.45(1)	0.01	25,740.67(4)[b]	0.01
10	25,817.90(4)[bw]	0.02	25,779.04(2)[b]	0.01	25,743.74(2)	0.01
11	25,828.68(3)[b]	0.02	25,786.305(7)	0.005	25,747.48(3)[b]	0.02
12	25,840.09(3)[bw]	−0.01	25,794.23(2)[b]	0.01	25,751.86(3)[b]	0.01
13	25,852.22(4)[bw]	0.03	25,802.80(2)[b]	0.01	25,756.93(2)[b]	0.01
14	25,864.96(2)	0.01	25,812.04(2)[b]	0.01	25,762.63(3)[b]	0.01
15	25,878.39(3)[bw]	0.03	25,821.939(8)	0.010	25,768.99(3)[b]	−0.02
16	25,892.44(5)[bw]	0.01	25,832.50(2)[b]	0.01	25,776.03(2)[b]	−0.02
17	25,907.19(3)[w]	0.02	25,843.71(2)[b]	0.01	25,783.76(3)[b]	0.01
18	25,922.57(5)[bw]	0.01	25,855.60(2)[b]	0.01	25,792.13(3)[b]	0.02
19	25,938.65(4)[bw]	0.03	25,868.16(2)[b]	0.03	25,801.16(2)[b]	0.02
20	25,955.33(7)[bw]	−0.01	25,881.35(2)[b]	0.01	25,810.85(2)	0.01
21	25,972.71(3)[w]	0.02	25,895.22(3)[b]	0.01	25,821.22(3)[b]	0.02
22			25,909.75(2)[b]	0.01	25,832.23(3)[bw]	0.01
23			25,924.95(4)[bw]	0.01	25,843.90(5)[bw]	−0.03
24			25,940.82(4)[bw]	0.01	25,856.28(5)[bw]	−0.02
25			25,957.36(4)[bw]	−0.01	25,869.36(3)[bw]	0.02
26			25,974.58(4)[bw]	−0.01	25,883.06(4)[bw]	−0.01
27			25,992.49(4)[bw]	−0.01	25,897.47(3)[bw]	−0.01
28			26,011.28(5)[bw]	0.02	25,912.77(4)[bw]	0.03
29			26,029.68(3)[w]	0.01		

[a] In cm^{-1}. *o–c* mean the observed minus calculated values. The instrumental resolution was 0.018 cm^{-1}. The estimated absolute calibration uncertainty was 0.004 cm^{-1}. The uncertainties in parentheses indicate 1σ standard deviations being combinations of fitting and calibration errors. The absolute accuracy of the line frequency measurements was estimated to ca. 0.04 cm^{-1}.
[b] Lines marked with *b* and/or *w* are blended and/or weak.

Table 3
Wavenumbers of the interaction-induced lines observed in VIS-FT emission bands in $^{13}C^{18}O$. [a,b,c]

J″	$^sR_{11ee}$	o–c	$^rR_{12ef}$	o–c	$^qQ_{11ef}$	o–c	$^qQ_{12ef}$	o–c
				$B^1\Sigma^+$ - $d^3\Delta$ (0, 6)				
45	21,620.00(2)[w]	0.01						
46							21,418.69(4)[w]	0.04
47			21,646.63(5)[w]	−0.05				
48							21,549.47(4)[bw]	−0.02
				$B^1\Sigma^+$ - $D^1\Delta$ (0, 1)				
28					21,001.69 (1)[w]	0.01		

[a] In cm^{-1}. *o–c* mean the observed minus calculated values. The uncertainties in parentheses indicate 1σ standard deviations being combinations of fitting and calibration errors.
[b] Lines marked with *b* and/or *w* are blended and/or weak.
[c] The superscripts *q*, *r* and *s* mean change in the quantum number of total angular momentum excluding spin (***N***).

(RMSE) of unweighted residuals of all reference wavenumbers in the final fit is 0.0092 cm^{-1} and within the measurement uncertainties, giving us confidence in the precision and quality of the fitted model.

Finally, $A^1\Pi(v = 1)$ and its perturbers were described by 23 molecular parameters, i.e.: the $A^1\Pi(v = 1)$, $d^3\Delta(v = 6)$, $e^3\Sigma^-(v = 3)$, $D^1\Delta(v = 1)$, $I^1\Sigma^-(v = 2)$ molecular constants; the $A^1\Pi(v = 1) \sim [d^3\Delta(v = 6), e^3\Sigma^-(v = 3), a'\,^3\Sigma^+(v = 11)]$ and $a^3\Pi(v = 12) \sim [D^1\Delta(v = 1), I^1\Sigma^-(v = 2)]$ spin–orbit perturbation parameters; the $A^1\Pi(v = 1) \sim [D^1\Delta(v = 1), I^1\Sigma^-(v = 1, 2)]$ rotation-electronic (***L***-uncoupling) perturbation parameters; the $a^3\Pi(v = 12) \sim [d^3\Delta(v = 5)]$ spin–orbit/spin-electronic/***L***-uncoupling perturbation parameter. Simultaneously, the $B^1\Sigma^+(v = 0)$ and $C^1\Sigma^+(v = 0)$ states were represented by 112 terms. The molecular parameters are gathered in Table 9. The experimental term values of $B^1\Sigma^+(v = 0)$ and $C^1\Sigma^+(v = 0)$ levels are listed in Table 10, whilst terms of $A^1\Pi(v = 1)$, $e^3\Sigma^-(v = 3)$, $I^1\Sigma^-(v = 2)$, $D^1\Delta(v = 1)$ and $d^3\Delta(v = 6)$ are grouped in Table 11. Fig. 5 shows the reduced terms of the $A^1\Pi(v = 1)$ level and its perturbers. Full details of the final deperturbation can be found in the output (*.log) file of PGOPHER program attached as supplementary material.

Intra-molecular interactions affecting the nominal $A^1\Pi(v = 1)$ and $a^3\Pi(v = 12)$ reduce $^1\Pi$ and $^3\Pi$ characters which, as a percentage, is equal to $C_{ik}^2 \cdot 100\,\%$, where $C_{ik} = \langle\Phi_k|\psi_i\rangle$ is the mixing coefficient resulting from the diagonalization of uncoupled Hunds-case (a) levels Φ_i and ψ_i. The mixed-state $^1\Pi$ percentage-character is listed in Table 11 for the main perturbers of $A^1\Pi(v = 1)$. The $^1\Pi$ and $^3\Pi$ percentage character for all modelled states and borrowing of $^3\Pi$ character in $^1\Pi$ and vice versa, illustrating the indirect interaction of $a^3\Pi(v = 12)$ and $A^1\Pi(v = 1)$ in $^{13}C^{18}O$, are presented in Fig. 6.

Machine readable copies (in ASCII format) of Tables 1-7 and Table 9 are included in the supplementary material.

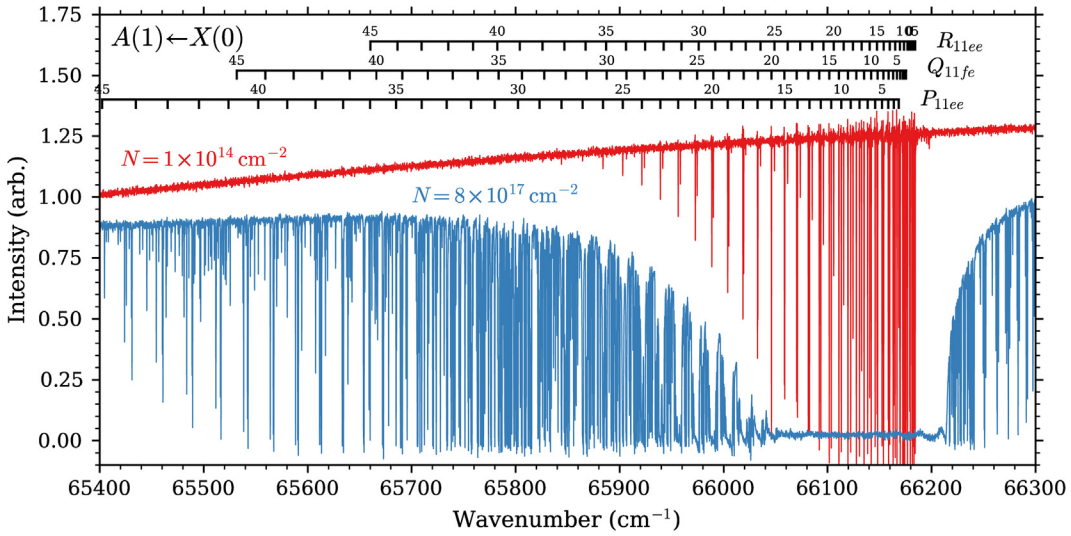

Fig. 3. SOLEIL absorption spectra showing $^{13}C^{18}O$ A(1) ← X(0) at two column densities. Many other transitions are visible in the high column density spectrum (N = 8 × 10^{17}cm^{-2}) arising from forbidden transitions and contamination by the A(1) ← X(0) bands of $^{12}C^{16}O$, $^{12}C^{18}O$, and $^{13}C^{17}O$.

Table 4
Wavenumbers of the VUV-FT $A^1\Pi$ - $X^1\Sigma^+(1, 0)$ absorption band in $^{13}C^{18}O$.[a,b]

J″	R(J″)	o–c	Q(J″)	o–c	P(J″)	o–c
0	66,178.94(1)	0.01	–	–	–	–
1	66,181.20(1)	0.01	66,175.45(1)	0.01	–	–
2	66,182.83(1)	0.01	66,174.21(1)	0.01	66,168.46(1)	0.01
3	66,183.84(1)[b]	0.01	66,172.35(1)	0.01	66,163.73(1)	0.01
4	66,184.23(1)[b]	0.01	66,169.87(1)	0.01	66,158.38(1)	0.01
5	66,184.00(1)[b]	0.01	66,166.77(1)	0.01	66,152.41(1)	0.01
6	66,183.15(1)	0.01	66,163.05(1)	0.01	66,145.82(1)	0.01
7	66,181.68(1)	0.01	66,158.71(1)	0.01	66,138.61(1)	0.01
8	66,179.59(1)	0.01	66,153.75(1)	0.01	66,130.78(1)	0.01
9	66,176.88(1)	0.01	66,148.18(1)	0.01	66,122.33(1)	0.01
10	66,173.55(1)	0.01	66,141.98(1)	0.01	66,113.27(1)	0.01
11	66,169.60(1)	0.01	66,135.16(1)	0.01	66,103.58(1)	0.01
12	66,165.03(1)	0.01	66,127.72(1)	0.01	66,093.28(1)	0.01
13	66,159.83(1)	0.01	66,119.67(1)	0.01	66,082.36(1)	0.01
14	66,154.01(1)	0.01	66,110.99(1)	0.01	66,070.82(1)	0.01
15	66,147.57(1)	0.01	66,101.69(1)	0.01	66,058.66(1)	0.01
16	66,140.51(1)	0.01	66,091.77(1)	0.01	66,045.89(1)	0.01
17	66,132.82(1)	0.01	66,081.23(1)	0.01	66,032.49(1)	0.01
18	66,124.50(1)	0.01	66,070.06(1)	0.01	66,018.47(1)	0.01
19	66,115.57(1)	0.01	66,058.28(1)	0.01	66,003.84(1)	0.01
20	66,106.00(1)	0.01	66,045.87(1)	0.01	65,988.58(1)	0.01
21	66,095.81(1)	−0.01	66,032.83(1)	0.01	65,972.71(1)	0.01
22	66,084.99(1)	−0.01	66,019.17(1)	0.01	65,956.21(1)	0.01
23	66,073.54(1)	0.01	66,004.89(1)	0.01	65,939.09(1)	−0.01
24	66,061.45(2)	0.01	65,989.97(1)	0.01	65,921.35(1)	−0.01
25	66,048.74(2)	0.02	65,974.43(1)	0.01	65,902.99(1)	0.01
26	66,035.35(2)	0.01	65,958.26(2)	0.02	65,883.99(2)	0.01
27	66,021.14(2)	−0.01	65,941.42(2)	0.02	65,864.37(2)[b]	0.02
28	66,007.35(2)[w]	0.02	65,923.74(2)	−0.01	65,844.09(2)	0.01
29	65,991.83(2)[w]	−0.01	65,906.49(2)[b]	0.01	65,822.98(2)[b]	−0.01
30	65,975.92(2)[w]	0.01	65,887.54(2)[b]	0.02	65,802.32(2)	0.02
31	65,959.39(2)[b]	−0.01	65,868.15(2)[b]	0.01	65,779.91(2)	−0.01
32	65,942.24(2)[b]	0.01	65,848.14(2)[b]	−0.01	65,757.13(2)[b]	0.01
33	65,924.46(2)[b]	0.01	65,827.50(2)[b]	0.01	65,733.74(2)[b]	−0.01
34	65,906.04(2)[b]	0.01	65,806.13(2)	−0.01	65,709.74(2)	0.01
35	65,886.96(2)[b]	−0.01	–	–	65,685.11(2)[b]	0.01
36	65,867.26(2)	0.02	65,763.63(2)	0.01	65,659.85(2)	0.01
37	65,846.87(2)[b]	−0.01	65,739.56(2)[b]	−0.01	65,633.94(2)[b]	−0.01
38	65,825.84(2)	0.01	65,715.58(2)[b]	−0.03	65,607.43(2)	0.02
39	65,804.03(2)	0.01	–	–	65,580.23(2)[b]	−0.01
40	65,782.40(3)	0.03	65,666.04(2)	0.04	65,552.40(2)	0.01
41			65,640.24(2)	0.01	65,523.79(2)	0.01
42			65,613.74(3)	−0.01	65,495.38(3)[w]	0.03
43			65,586.36(6)[w]	−0.01		

[a] In cm^{-1}. *o–c* mean the observed minus calculated values. The instrumental resolution was 0.15 cm^{-1}. The estimated absolute calibration uncertainty was 0.01 cm^{-1}. The uncertainties in parentheses indicate 1σ standard deviations being combinations of fitting and calibration errors. The absolute accuracy of the line frequency measurements was estimated to fall between 0.01 and 0.06 cm^{-1}, depending on the line intensity and blending.

[b] Lines marked with *b* and/or *w* are blended and/or weak.

Table 5
Wavenumbers of the interaction-induced lines observed in the $A^1\Pi$ - $X^1\Sigma^+(1, 0)$ VUV-FT absorption spectra in $^{13}C^{18}O$.[a,b,c]

J''	$^qQ_{11fe}$	o–c	$^pP_{11ee}$	o–c	$^qQ_{21fe}$	o–c	$^qR_{11ee}$	o–c	$^rR_{21ee}$	o–c
					$D^1\Delta$ – $X^1\Sigma^+(1, 0)$					
27	65,969.15(5)[b]	−0.01								
28	65,934.34(5)[b]	0.03					65,997.85(3)[b]	0.04		
29	65,897.00(5)	−0.01	65,833.51(5)[b]	−0.01			65,963.92(5)	0.01		
30	65,859.68(3)	0.01	65,792.77(5)	−0.01			65,928.51(5)[b]	0.01		
31			65,751.99(3)[b]	−0.01			65,891.76(5)[b]	−0.03		
32										
					$e^3\Sigma^-$ – $X^1\Sigma^+(3, 0)$					
39					65,822.01(2)	−0.01				
...										
42							65,664.65(2)	−0.01		
...										
45					65,497.05(2)	0.01				
					$d^3\Delta$ – $X^1\Sigma^+(6, 0)$					
43					65,723.37(2)[b]	0.01				
...										
46									65,650.33(2)[w]	0.01

[a] In cm^{-1}. The uncertainties in parentheses indicate 1σ standard deviations being combinations of the fitting and calibration errors.
[b] Lines marked with *b* and/or *w* are blended and/or weak.
[c] The superscripts *p*, *q* and *r* denote change in the total angular momentum excluding spin.

4. Discussion and conclusions

Haridass et al. [27] takes into account only 3 interactions affecting $A^1\Pi(v = 1)$ in $^{13}C^{18}O$, i.e. $A(v = 1) \sim [D(v = 1), a'(v = 10), d(v = 5)]$, with the first two floated in their final fit. The current analysis, based on a more comprehensive and accurate experimental data set permitted the investigation of 38 interactions suspected of perturbing of the $A(v = 1)$ level. As many as 21 of which proved to be significant given the accuracy of line frequencies, and 9 interaction parameters are floated in the final fit. The significant interactions include previously known $A(v = 1) \sim [D(v = 1), a'(v = 10), d(v = 5)]$ perturbations and newly-modelled *(i)* direct $A(v = 1) \sim [d(v = 6), e(v = 2), e(v = 3), a'(v = 11)]$ spin–orbit interactions and $A(v = 1) \sim [I(v = 1), I(v = 2)]$ rotation-electronic perturbations; *(ii)* indirect $a(v = 12) \sim [e(v = 2), e(v = 3), d(v = 5), d(v = 6)] \sim A(v = 1)$ spin–orbit/spin-electronic/***L***–uncoupling and spin–orbit interactions; $a(v = 12) \sim [I(v = 2), D(v = 1)] \sim A(v = 1)$ spin–orbit and ***L***–uncoupling interactions as well as the $d(v = 5) \sim a'(v = 10) \sim A(v = 1)$ and $d(v = 6) \sim a'(v = 11) \sim A(v = 1)$ spin–spin/spin–orbit perturbations (see Table 8 and Table 9). It means that the indirect influence of $a^3\Pi$ on the $A^1\Pi$ state results from two pairs of well-determined perturbation parameters: $\eta_{a(12)\sim D(1)} = -3.47(17)$ cm^{-1} and $\xi_{D(1)\sim A(1)} = -6.6526(227) \times 10^{-2}$ cm^{-1} as well as $\eta_{a(12)\sim I(2)} = -8.5101(430)$ cm^{-1} and $\xi_{I(2)\sim A(1)} = -7.758(12) \times 10^{-2}$ cm^{-1}. The indirect $a^3\Pi(v = 12) \sim A^1\Pi(v = 1)$ interaction is not detectable by the observation of intensity anomalies or level shifts. This is because of the intensity of optically-forbidden transitions to perturbed $a^3\Pi$ levels are a factor of $10^3 - 10^4$ weaker than corresponding transitions to $A^1\Pi$. Such detection is only possible thanks to the precise fit of multiple direct perturbations that is taken here to a new level.

Fig. 5 shows reduced terms of $^{13}C^{18}O$ $A^1\Pi(v = 1)$ that are significantly perturbed by the $D^1\Delta(v = 1)$, $I^1\Sigma^-(v = 2)$ singlet states and $e^3\Sigma^-(v = 3)$, $a'^3\Sigma^+(v = 11)$, $d^3\Delta(v = 6)$, $a^3\Pi(v = 12)$ triplet states where their rotational level energies are nearly degenerate. The largest shift, 1.4 cm^{-1}, occurs near the anti-crossing of the $A^1\Pi$ $(v = 1)$ F_{1f} component and $I^1\Sigma^-(v = 2)$ at $J = 36$ as a result of a rotation-electronic coupling. The shift of the $A^1\Pi(v = 1)$ F_{1e} level at $J = 28$ is caused by $D^1\Delta(v = 1)$ and the same kind of interaction but is lesser in magnitude (about 0.4 cm^{-1}) despite the similar distance between the unperturbed levels (8.3 cm^{-1}) as for $A^1\Pi(v = 1) \sim I^1\Sigma^-(v = 2)$ (9.3 cm^{-1}) and similar-magnitude rotational operator integrals: $\left\langle v_{A(1)} \middle| \widehat{\boldsymbol{B}(\boldsymbol{R})} \middle| v_{I(2)} \right\rangle = 0.41$ cm^{-1}, $\left\langle v_{A(1)} \middle| \widehat{\boldsymbol{B}(\boldsymbol{R})} \middle| v_{D(1)} \right\rangle = 0.47$ cm^{-1}. The reasons for this difference are: *(i)* the interactions are *J*-dependent; *(ii)* the nearby $a^3\Pi$ $(v = 12)$ level is spin–orbit coupled to $D^1\Delta(v = 1)$ at $J = 28$ and this shifts it away from $A^1\Pi(v = 1)$ by about 0.82 cm^{-1}, indirectly weak-

Table 6
Wavenumbers of the VUV-FT $I^1\Sigma^-$ - $X^1\Sigma^+(2, 0)$ absorption bfand in $^{13}C^{18}O$.[a,b.]

J''	$Q(J'')$	o–c
3	66,588.1(2)[w]	0.1
4	66,583.09(6)	0.01
5	66,576.76(4)	−0.01
6	66,569.18(3)	0.01
7	66,560.34(2)	0.01
8	66,550.23(2)	−0.01
9	66,538.86(2)	0.01
10	66,526.22(2)	−0.01
11	66,512.33(2)	−0.01
12	66,497.16(2)	−0.01
13	66,480.74(2)	−0.01
14	66,463.05(2)	−0.01
15	66,444.10(2)	0.01
16	66,423.87(2)	−0.01
17	66,402.39(2)	−0.01
18	66,379.64(2)[b]	−0.01
19	66,355.64(2)	0.01
20	66,330.36(2)	0.01
21	66,303.82(2)[b]	−0.01
22	66,276.02(2)	0.01
23	66,246.96(2)	0.01
24	66,216.66(5)[b]	0.02
...	–	–
32	65,928.98(1)[w]	−0.01
...	–	–
35	65,798.91(5)[b]	−0.01
36	65,751.22(5)[b]	0.02

[a] In cm^{-1}. *o–c* mean the observed minus calculated values. The instrumental resolution was 0.15 cm^{-1}. The estimated absolute calibration uncertainty was 0.01 cm^{-1}. The uncertainties in parentheses indicate 1σ standard deviations being combinations of fitting and calibration errors. The absolute accuracy of the line frequency measurements was estimated to fall between 0.02 and 0.05 cm^{-1} depending on the line intensity and blending.
[b] Lines marked with *b* and/or *w* are blended and/or weak.

Table 7
Wavenumbers of the VUV-FT $C^1\Pi$ - $X^1\Sigma^+(0, 0)$ absorption band in $^{13}C^{18}O$.[a,b]

J″	R(J″)	o–c	P(J″)	o–c
0	91,922.35(2)	−0.01	–	–
1	91,925.92(2)	−0.01	91,915.32(2)	0.01
2	91,929.53(2)	0.01	91,911.87(2)	−0.01
3	91,933.18(2)	−0.01	91,908.46(2)	−0.01
4	91,936.88(2)	−0.01	91,905.08(2)	0.01
5	91,940.61(2)	−0.01	91,901.75(2)	−0.01
6	91,944.38(2)	−0.01	91,898.46(2)	−0.01
7	91,948.19(2)	−0.01	91,895.21(2)	−0.01
8	91,952.03(2)	−0.01	91,892.00(2)	−0.01
9	91,955.92(2)	−0.01	91,888.83(2)	−0.01
10	91,959.85(2)	−0.01	91,885.71(2)	−0.01
11	91,963.82(2)	−0.01	91,882.62(2)	−0.01
12	91,967.81(2)	−0.01	91,879.57(2)	−0.01
13	91,971.86(2)	−0.01	91,876.57(2)	−0.01
14	91,975.93(2)	−0.01	91,873.61(2)	−0.01
15	91,980.05(2)	−0.01	91,870.69(2)	−0.01
16	91,984.21(2)	−0.01	91,867.81(2)	−0.01
17	91,988.40(2)	−0.01	91,864.97(2)	−0.01
18	91,992.63(2)	−0.01	91,862.17(2)	−0.01
19	91,996.89(2)	−0.01	91,859.42(2)	−0.01
20	92,001.20(2)	−0.01	91,856.71(2)	−0.01
21	92,005.54(2)	−0.01	91,854.04(2)	−0.01
22	92,009.92(2)	0.01	91,851.41(2)	−0.01
23	92,014.34(2)	−0.01	91,848.82(2)	−0.01
24	92,018.80(2)	0.01	91,846.28(2)	0.01
25	92,023.28(2)	0.01	91,843.79(2)	−0.01
26	92,027.81(2)	−0.01	91,841.33(2)	0.01
27	92,032.37(2)	−0.01	91,838.92(2)	0.01
28	92,036.96(2)	−0.01	91,836.54(2)	−0.01
29	92,041.59(2)	−0.01	91,834.21(2)	−0.01
30	92,046.26(2)	−0.01	91,831.92(2)	−0.01
31	92,050.96(2)	−0.01	91,829.68(2)	0.01
32	92,055.70(2)	0.01	91,827.47(2)	0.01
33	92,060.47(2)	−0.01	91,825.31(2)	0.01
34	92,065.27(2)	0.01	91,823.20(2)	−0.01
35	92,070.11(2)	0.01	91,821.12(2)	0.01
36	92,074.99(2)	0.01	91,819.09(2)	−0.01
37	92,079.89(2)	−0.01	91,817.10(2)	−0.01
38	92,084.83(2)	−0.01	91,815.15(2)	−0.01
39	92,089.81(2)	0.01	91,813.25(2)	0.01
40	92,094.82(2)	−0.01	91,811.39(2)	0.01
41	92,099.87(2)	−0.01	91,809.57(2)	−0.01
42	92,104.94(2)	−0.01	91,807.80(2)	0.01
43	92,110.05(2)	−0.01	91,806.07(2)	0.01
44	92,115.19(2)	−0.01	91,804.38(2)	0.01
45	92,120.37(2)	−0.01	91,802.74(2)	0.01
46	92,125.56(2)	−0.01	91,801.14(2)	0.01
47	92,130.80(2)	−0.01	91,799.59(2)	0.01
48	92,136.07(2)	−0.01	91,798.06(2)	0.01
49	92,141.37(2)	−0.01	91,796.60(2)	0.01
50	92,146.69(2)	−0.01	91,795.17(2)	0.01
51	92,152.04(2)	−0.01	91793.79(2)	0.01
52	92,157.44(2)	−0.01	91,792.43(2)	0.01
53	92,162.87(3)	−0.01	91,791.12(2)	0.01
54	92,168.31(3)	−0.01	91,789.87(2)	0.01
55	92,173.76(4)	−0.01	91,788.67(3)[w]	0.01
56	92,179.29(5)	−0.01	91,787.49(3)[w]	0.01
57	92,184.84(6)[w]	−0.01	91,786.33(4)[w]	0.01
58	92,190.37(7)[w]	−0.01	91,785.27(5)[w]	0.01
59	92,196.0(1)[w]	−0.1	91,784.24(6)[w]	0.01
60			91,783.19(7)[w]	0.01
61			91,782.3(1)[w]	0.1

[a] In cm^{-1}. *o–c* mean the observed minus calculated values. The instrumental resolution was between 0.15 and 0.32 cm^{-1}. The estimated absolute calibration uncertainty was 0.01 cm^{-1}. The uncertainties in parentheses indicate 1σ standard deviations being combinations of fitting and calibration errors. The absolute accuracy of the line frequency measurements was estimated to fall between 0.02 and 0.1 cm^{-1} depending on the line intensity and blending.

[b] Lines marked with *b* and/or *w* are blended and/or weak.

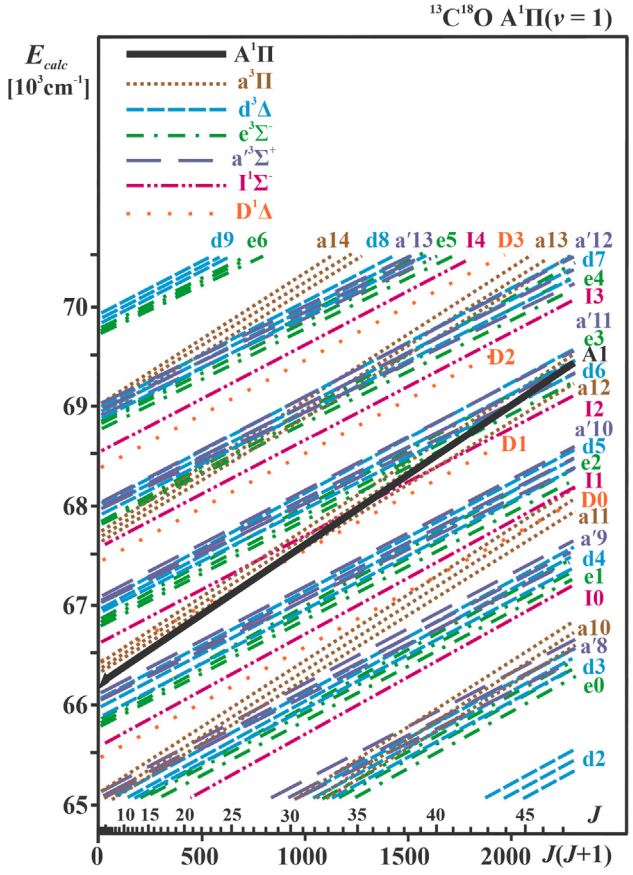

Fig. 4. The ro-vibrational terms diagram of the $^{13}C^{18}O$ $A^1\Pi(v = 1)$ level and its energy surrounding in the 65,000–75,000 cm^{-1} region.

ening the $A^1\Pi(v = 1) \sim D^1\Delta(v = 1)$ interaction. To confirm that the apparent indirect influence of $a^3\Pi(v = 12)$ on $A^1\Pi(v = 1)$ deduced here is not an alias for the other direct interactions we have modified the PGOPHER model while leaving out $a^3\Pi$ entirely. The residual of this reduced model is ten-times greater than when $a^3\Pi$ is included and the pattern of *J*-dependent residuals, plotted in supplementary material (Figs. S1 – S3), is clearly non-normal.

The pure $^1\Pi$ percentage character of perturbed $A^1\Pi(v = 1, F_{1e,f}, |\Omega| = 1)$ levels, as shown in Fig. 6 and Table 11, is least near avoided crossings with *(i)* the $e^3\Sigma^-(v = 3, F_{2f}, |\Omega| = 1)$ and $d^3\Delta(v = 6, F_{1f}, F_{2f}, F_{3f}, |\Omega| = 3, 2, 1)$ levels at $J = 44$ and equals 81% and 54% for *e* and *f* components of $A^1\Pi(v = 1)$, respectively; *(ii)* the $I^1\Sigma^-(v = 2, |\Omega| = 0)$ level at $J = 36$ and is 88%; *(iii)* the $D^1\Delta(v = 1, F_{1e,f}, |\Omega| = 2)$ levels at $J = 29$ and equals 95%; *(iv)* $e^3\Sigma^-(v = 3, F_{1e}, |\Omega| = 1)$ level at $J = 41$ and is 96%. Extrapolating the fitted model predicts that overlapping of Λ-components of same levels at $J = 47$, i.e. $a'^3\Sigma^+(v = 11, F_{2e}, |\Omega| = 1)$, $d^3\Delta(v = 6, F_{3e}, |\Omega| = 1)$ and $d^3\Delta(v = 6, F_{1e}, |\Omega| = 3)$, should result in $A^1\Pi(v = 1)$ character level as low as 47%, and 81% for the *e* and *f* components, respectively. Thus, it should occur the loss of the prevailing $^1\Pi$ character of $A^1\Pi(v = 1)$ for *e* component at $J = 47$. However, this range lies outside the current experimental data for $A^1\Pi$ $(v = 1)$. In turn, the $^3\Pi$ percentage character of the $a^3\Pi(v = 12, F_{1\text{-}3e,f}, |\Omega| = 0, 1, 2)$ level is decreasing mostly near avoided crossings with *(i)* the $D^1\Delta(v = 1, F_{1e,f}, |\Omega| = 2)$ levels at $J = 13, 20, 28$ down to 76% and 90%, 99% and 77%, 88% and 76% for the *e* and *f* parity, respectively; *(ii)* the $I^1\Sigma^-(v = 2, F_{1f}, |\Omega| = 0)$ level at $J = 27, 33, 40$ down to 76%, 88% and 79%, respectively; *(iii)* the $e^3\Sigma^-(v = 3, F_{2f}, |\Omega| = 1)$ level at $J = 40$ down to 79%; *(iv)* the $e^3\Sigma^-(v = 3, F_{1e}, F_{3e}, |\Omega| = 1, 0)$ level at $J = 41, 45, 47$ down to 81%, 72% and 87%, respectively; *(v)* the $d^3\Delta$ $(v = 6, F_{1\text{-}3e,f}, |\Omega| = 3, 2, 1)$ levels at $J = 41, 45$–$46, 50$ down to 81%, 72–74%, 82% and 82%, 74%-83%, 82% for *e* and *f* component, respectively.

The $a^3\Pi(v = 12)$ level does not directly interact with $A^1\Pi(v = 1)$ due to their negligible Franck-Condon factor (2.38×10^{-9}). In our

Table 8
Interactions tested within the $A^1\Pi(v = 1)$ deperturbation analysis in $^{13}C^{18}O$.

N^o	Interactions			Nature of the perturbation	Part of the final fit	Status	Characteristics[a]
1	$A^1\Pi(v = 1)$	~	$D^1\Delta(v = 0)$	Rotation-electronic	No	-	Irrelevant.
2	"	~	$D^1\Delta(v = 1)$	"	Yes	Floated	–
3	"	~	$D^1\Delta(v = 2)$	"	No	–	Irrelevant.
4	"	~	$I^1\Sigma^-(v = 0)$	"	No	–	Irrelevant.
5	"	~	$I^1\Sigma^-(v = 1)$	"	Yes	Floated	–
6	"	~	$I^1\Sigma^-(v = 2)$	"	Yes	Floated	–
7	"	~	$I^1\Sigma^-(v = 3)$	"	No	–	Irrelevant.
8	"	~	$e^3\Sigma^-(v = 1)$	Spin-orbit	No	–	Irrelevant.
9	"	~	$e^3\Sigma^-(v = 2)$	"	Yes	Fixed	Noticeable. If floated, it correlates among others with < A(1)|$\mathbf{J^+L^-}$|D(1) > and T, B constants of A(1).
10	"	~	$e^3\Sigma^-(v = 3)$	"	Yes	Floated	–
11	"	~	$e^3\Sigma^-(v = 4)$	"	No	–	Irrelevant.
12	"	~	$d^3\Delta(v = 4)$	"	No	–	Irrelevant.
13	"	~	$d^3\Delta(v = 5)$	"	Yes	Fixed	Noticeable. If floated, it correlates with T, B, D constants of A(1).
14	"	~	$d^3\Delta(v = 6)$	"	Yes	Floated	–
15	"	~	$d^3\Delta(v = 7)$	"	No	–	Irrelevant.
16	"	~	$a'^3\Sigma^+(v = 9)$	"	No	–	Irrelevant.
17	"	~	$a'^3\Sigma^+(v = 10)$	"	Yes	Fixed	Noticeable. If floated, it correlates with T, B constants of A(1).
18	"	~	$a'^3\Sigma^+(v = 11)$	"	Yes	Floated	–
19	"	~	$a'^3\Sigma^+(v = 12)$	"	No	–	Irrelevant.
20	$e^3\Sigma^-(v = 2)$	~	$a'^3\Sigma^+(v = 10)$	"	No	–	Statistically unjustified. No theoretical value available.
21	$e^3\Sigma^-(v = 3)$	~	$a'^3\Sigma^+(v = 11)$	"	No	–	Statistically unjustified. No theoretical value available.
22	$d^3\Delta(v = 5)$	~	$a'^3\Sigma^+(v = 10)$	Spin-spin	Yes	Fixed[b]	Noticeable. Statistically unjustified.
23	$d^3\Delta(v = 6)$	~	$a'^3\Sigma^+(v = 11)$	"	Yes	Fixed[b]	Noticeable. Statistically unjustified.
24	"	~	$e^3\Sigma^-(v = 3)$	"	No	–	Noticeable. If floated, it correlates with < A(1)|$\mathbf{LS}$|d(6) >. No theoretical value available.
25	$a^3\Pi(v = 12)$	~	$D^1\Delta(v = 1)$	Spin-orbit	Yes	Floated	–
26	"	~	$I^1\Sigma^-(v = 2)$	"	Yes	Floated	–

(*continued on next page*)

Table 8 (*continued*)

N^o	Interactions			Nature of the perturbation	Part of the final fit	Status	Characteristics[a]
27	"	~	$e^3\Sigma^-(v=2)$	Spin-orbit / spin-electronic Rotation-electronic	Yes	Fixed	Noticeable. Statistically unjustified.
28	"	~	"		Yes	Fixed	Noticeable. Statistically unjustified.
29	"	~	$e^3\Sigma^-(v=3)$	Spin-orbit / spin-electronic Rotation-electronic	Yes	Fixed	Noticeable. If floated, it correlates with < A(1)|**LS**|d(6) > and T, B of e(3).
30	"	~	"		Yes	Fixed	Noticeable. Statistically unjustified.
31	"	~	$d^3\Delta(v=5)$	Spin-orbit / spin-electronic Rotation-electronic	Yes	Floated	–
32	"	~	"		Yes	Fixed	Noticeable. If floated, it correlates with < a(12)|**LS**|d(5) >.
33	"	~	$d^3\Delta(v=6)$	Spin-orbit / spin-electronic Rotation-electronic	Yes	Fixed	Noticeable. If floated, it correlates with A constant of d(6).
34	"	~	"		Yes	Fixed	Noticeable. If floated, it correlates with T,B, and A constants of d(6) as well as causes many other significant correlations.
35	"	~	$a'^3\Sigma^+(v=10)$	Spin-orbit / spin-electronic Rotation-electronic	No	–	Irrelevant.
36	"	~	"		No	–	Irrelevant.
37	"	~	$a'^3\Sigma^+(v=11)$	Spin-orbit / spin-electronic Rotation-electronic	No	–	Irrelevant.
38	"	~	"		No	–	Irrelevant.

[a] "Noticeable" means influence of the perturbation parameters on the values of the: *(i)* molecular constants and/or *(ii)* interactions within one standard deviation and/or *(iii)* residual within accuracy of the experimental lines used in the final deperturbation fit. The individual significance was tested via verifying of the result differences of the appropriate quantities using floated or fixed to the calculated value (and then to zero) interaction parameter.

[b] Calculated in this work on the basis of the $\epsilon_{v'v''}/\langle v'|v''\rangle = const$ dependence as well as $\epsilon_{a'(9)d(4)}$ taken form Hakalla et al. [17] within the same isotopologue ($^{13}C^{18}O$).

Table 9
Deperturbed molecular constants of the $^{13}C^{18}O$ $A^1\Pi(v=1)$ and perturber levels as well as their interaction parameters.[a,b]

Constant	$A^1\Pi(v=1)$	$A^1\Pi(v=1)$from Ref. [27]	$d^3\Delta(v=5)$	$d^3\Delta(v=6)$	$e^3\Sigma^-(v=2)$	$e^3\Sigma^-(v=3)$	
T_v	66,175.533 58(143)	66,175.608(7)[d]	65,949.55[e]	66,956.980 10(7930)	65,802.44[e]	66,811.029 3(299)	
B	1.437 635 35(313)	1.437 49(5)[d]	1.11[f]	1.094 152 90(4067)	1.13[f]	1.112 690 1(164)	
$D \times 10^6$	6.139 67(210)	6.6(1)[d]	5.33[g]	5.31[g]	5.58[g]	5.55[g]	
$H \times 10^{12}$	−12.81[c]		−0.60[f]	−0.60[h]	−1.50[h]	−1.50[h]	
A			−16.69[f]	−16.061(22)			
$A_D \times 10^5$			−9.17[i]	−9.17[i]			
λ			0.89[f]	0.99[f]	0.57[f]	0.524 5(70)	
$\gamma \times 10^2$			0.69[i]	0.76[i]			
$\eta(A^1\Pi_{v=1} \sim v^{"})$			15.57[o]	18.112 2(403)	14.05[o]	−5.405 9(303)	
$\eta(a^3\Pi_{v=12} \sim v^{"})$[p]			47.73 (662)	26.31	5.09	8.24	
$[\xi(a^3\Pi_{v=12} \sim v^{"}) \times 10^2]$[q]			7.00	−5.80	1.00	1.60	
Constant	$D^1\Delta(v=1)$	$D^1\Delta(v=1)$ from Ref. [27]	$I^1\Sigma^-(v=1)$	$I^1\Sigma^-(v=2)$	$a^3\Pi(v=12)$	$a'^3\Sigma^+(v=10)$	$a'^3\Sigma^+(v=11)$
T_v	66,442.929 8(422)	66,456.5(9)[d]	65,593.17[e]	66,595.534 88(449)	66,355.00[e]	66,066.95[e]	67,037.79[e]
B	1.120 160 7(487)	1.17246[d]	1.13[f]	1.114 621 0(220)	1.32[f]	1.07[f]	1.05[f]
$D \times 10^6$	5.79[j]	6.3[d]	5.67[h]	5.702 4(191)	5.67[g]	5.17[g]	5.16[g]
$H \times 10^{12}$	−0.22[h]		2.25[h]	2.25[h]		−0.30[h]	−0.30[h]
A					38.79[f]		
$A_D \times 10^5$					−20.58[k]		
$\lambda \times 10^2$					−0.51[k]	−114.80[f]	−114.20[f]
$\gamma \times 10^2$					0.33[i]	−0.51[i]	−0.50[i]
o					0.67[l]		
$p \times 10^3$					2.73[m]		
$q \times 10^5$					2.95[n]		
$\eta(A^1\Pi_{v=1} \sim v^{"})$						−5.29[o]	3.593(284)

Table 9 (*continued*)

Constant	$D^1\Delta(v=1)$	$D^1\Delta(v=1)$ from Ref. [27]	$I^1\Sigma^-(v=1)$	$I^1\Sigma^-(v=2)$	$a^3\Pi(v=12)$	$a'^3\Sigma^+(v=10)$	$a'^3\Sigma^+(v=11)$
$\xi(A^1\Pi_{v=1}\sim v^{"})\times 10^2$	−6. 652 6(227)	−8.5(9)[s]	10.12(17)	−7.758(12)			
$\eta(a^3\Pi_{v=12}\sim v^{"})$[q]	−3.47(17)			−8.510 1(430)			
$\epsilon(d^3\Delta_{v=5}\sim v^{"})$[r]						0.18	
$\epsilon(d^3\Delta_{v=6}\sim v^{"})$[r]							−0.10

[a] In cm^{-1}.
[b] Numbers in parentheses are 1σ standard uncertainties in units of last-significant digit. When writing the results with their uncertainties, the approach described by Watson [59] was used to avoid a non-physical precision when recreating energy levels using data obtained in this work, so some uncertainty values were rounded to more than two significant digits.
[c] Calculated in this work on the basis of Ref. [20,21] and isotopic scaling procedure.
[d] In the present paper, the rotational operator in the effective Hamiltonian is expressed by the total angular momentum operator excluding spin ($\widehat{\boldsymbol{N}}$), as recommended by IUPAC [60], while the authors of a previous deperturbation analysis in Ref. [27] used the angular momentum of nuclear framework ($\widehat{\boldsymbol{R}}$). To compare the results, the values are converted to be expressed by ($\widehat{\boldsymbol{N}}$) operator. In general, the significant differences occur for the T_v and B constants by the value of BA^2 and $2DA^2$, respectively.
[e] Obtained by isotopic scaling of the combined values taken from Ref. [18] and Ref. [56].
[f] Calculated based on Ref. [18] and isotopic scaling procedure. Diagonal spin–spin constant $\lambda = -1.5 \times C$ (in MHz and converted into cm^{-1}).
[g] Calculated based on Ref. [18] and isotopic scaling procedure.
[h] Calculated in this work on the basis of Ref. [47] and isotopic scaling procedure.
[i] Taken from Ref. [18] (in MHz), then converted into cm^{-1} and isotopically scaled.
[j] Obtained by isotopic scaling of the values taken from Ref. [54].
[k] Calculated in this work on the basis of Ref. [55] (in MHz), then converted into cm^{-1} and isotopically scaled. The diagonal spin–spin constant $\lambda = 1.5 \times \varepsilon$.
[l] Calculated in this work on the basis of Ref. [19] ($o = C^5$) and isotopic scaling procedure.
[m] Calculated in this work on the basis of Ref. [55] ($p = 2 \times p +$) and isotopic scaling procedure.
[n] Calculated in this work on the basis of Ref. [19] ($q = 2 \times B_{0*}$) and isotopic scaling procedure.
[o] The spin–orbit and rotation-electronic interaction parameters were calculated on the basis of isotopologue-independent $\boldsymbol{a}_{\boldsymbol{A\sim d,e,a'}}$ and $\boldsymbol{b}_{\boldsymbol{A\sim D,I}}$ electronic parameters [24,47] based on the equations (1) - (5) and (1) - (3) from Ref. [24] and Ref. [26], respectively. The vibrational overlap integrals $\left\langle v_A|v_{a',e,d}\right\rangle$ and rotational operator integrals $\langle v_A|\boldsymbol{B}(\boldsymbol{R})|v_{I,D}\rangle$ were calculated as it was described in Refs. [24,25].
[p] The spin–orbit and rotation-electronic ($\boldsymbol{L}$-uncoupling) interaction parameters were obtained on the basis of the isotopologue-independent $\boldsymbol{a}_{\boldsymbol{a\sim e,d,a'}}$ and $\boldsymbol{b}_{\boldsymbol{a\sim e,d,a'}}$ parameters from [19]. The $\alpha_{a\sim e,d,a'}(\boldsymbol{a}_{\boldsymbol{a\sim e,d,a'}})$ and $\beta_{\boldsymbol{a\sim e,d,\ a'}}(\boldsymbol{b}_{\boldsymbol{a\sim e,d,a'}})$ dependences given in Refs. [16,19] were used in the calculations. The $\eta_{a\sim e,d,a'}(\alpha_{\ a\sim e,d,a'})$ and $\xi_{a\sim e,d,a'}(\beta_{a\sim e,d,a'})$ relationships resulted from symmetrized matrix elements of the $a^3\Pi \sim e^3\Sigma^-$, $d^3\Delta$, $a'^3\Sigma^+$ interactions. The vibrational overlap integrals $\left\langle v_a|v_{e,d,a'}\right\rangle$ and rotational operator integrals $\left\langle v_a|\boldsymbol{B}(\boldsymbol{R})|v_{e,d,a'}\right\rangle$ were calculated as it was described in Refs. [25,61]. Both, the spin–orbit and spin-electronic couplings show the same Ω-dependence, thus it is impossible to determine them independently. For this reason the $\eta_{a\sim e,d,a'}$ parameters represent a linear combinations both of these interactions.
[q] The spin–orbit interaction parameters were calculated on the basis of isotopologue-independent parameters: $\boldsymbol{a}_{\boldsymbol{a\sim I}}$ [19] $\boldsymbol{a}_{\boldsymbol{a\sim D}}$ [57]. The $\alpha_{a\sim I}(\boldsymbol{a}_{\boldsymbol{a\sim I}})$ and $\alpha_{a\sim D}(\boldsymbol{a}_{\boldsymbol{a\sim D}})$ perturbation parameter dependences given in Refs. [16,19] were used in the calculations. The $\eta_{a\sim I}(\alpha_{a\sim I})$ and $\eta_{a\sim D}(\alpha_{a\sim D})$ relationships resulted from symmetrized matrix elements of the $a^3\Pi \sim I^1\Sigma^-$ and $a^3\Pi \sim D^1\Delta$ interactions. The vibrational overlap integrals $\langle v_a|v_{I,D}\rangle$ were calculated as it was described in Refs. [25,61].
[r] The spin–spin off-diagonal interaction calculated on the basis of $\left\langle v_{d(4)}\left|\boldsymbol{H}^{\boldsymbol{SS}}\right|v_{a'(9)}\right\rangle$ from Ref. [17] and the $\epsilon_{v'v''}/\langle v'|v''\rangle = const$ dependence for the same isotopologue.
[s] Converted in this work by means of formula (4) (see text).

Table 10
Term values of the $B^1\Sigma^+(v=0)$ and $C^1\Sigma^+(v=0)$ levels in $^{13}C^{18}O$.[a,b,c]

J	$B^1\Sigma^+$(v = 0)	$C^1\Sigma^+$(v = 0)
0	86,917.357(5)	91,918.815(6)
1	86,920.899(3)	91,922.350(4)
2	86,927.980(2)	91,929.415(4)
3	86,938.598(2)	91,940.009(4)
4	86,952.753(2)	91,954.139(4)
5	86,970.449(2)	91,971.805(4)
6	86,991.681(2)	91,992.996(4)
7	87,016.450(2)	92,017.721(4)
8	87,044.755(2)	92,045.973(4)
9	87,076.595(2)	92,077.755(3)
10	87,111.967(2)	92,113.059(4)
11	87,150.872(2)	92,151.897(3)
12	87,193.310(2)	92,194.258(4)
13	87,239.274(2)	92,240.133(4)
14	87,288.766(2)	92,289.537(4)
15	87,341.784(2)	92,342.462(3)
16	87,398.324(2)	92,398.903(4)
17	87,458.346(2)	92,458.859(4)
18	87,521.967(2)	92,522.329(4)
19	87,589.073(2)	92,589.313(4)
20	87,659.685(2)	92,659.804(4)
21	87,733.809(2)	92,733.801(4)
22	87,811.443(2)	92,811.303(4)
23	87,892.583(2)	92,892.308(4)
24	87,977.225(2)	92,976.822(4)
25	88,065.366(2)	93,064.823(4)
26	88,157.007(2)	93,156.318(4)
27	88,252.143(2)	93,251.299(5)
28	88,350.762(2)	93,349.767(5)
29	88,452.871(2)	93,451.719(5)
30	88,558.457(2)	93,557.148(5)

(*continued on next page*)

Table 10 (*continued*)

J	$B^1\Sigma^+$(v = 0)	$C^1\Sigma^+$(v = 0)
31	88,667.517(2)	93,666.055(5)
32	88,780.053(2)	93,778.434(5)
33	88,896.073(2)	93,894.282(5)
34	89,015.548(2)	94,013.592(5)
35	89,138.501(3)	94,136.357(5)
36	89,264.867(3)	94,262.581(5)
37	89,394.713(3)	94,392.254(5)
38	89,528.003(3)	94,525.376(5)
39	89,664.743(4)	94,661.937(5)
40	89,804.873(4)	94,801.938(4)
41	89,948.483(5)	94,945.372(4)
42	90,095.482(5)	95,092.232(5)
43	90,245.929(6)	95,242.508(5)
44	90,399.795(6)	95,396.206(5)
45	90,557.049(7)	95,553.315(5)
46	90,717.748(8)	95,713.839(5)
47	90,881.76(1)	95,877.743(5)
48	91,049.18(2)	96,045.054(5)
49	91,220.05(2)	96,215.748(5)
50	91,394.20(2)	96,389.832(5)
51		96,567.277(6)
52		96,748.088(7)
53		96,932.284(7)
54		97,119.837(9)
55		97,310.72(2)
56		97,504.93(2)
57		97,702.53(2)
58		97,903.44(3)
59		98,107.62(3)
60		98,315.20(4)

[a] In cm^{-1}. All values are given in relation to the ground state $X^1\Sigma^+(v = 0, J = 0)$ level.
[b] Based on simultaneous fitting (so called *the term-value fitting approach*) of the $^{13}C^{18}O$ $B^1\Sigma^+(v = 0)$ and $C^1\Sigma^+(v = 0)$ term values, molecular constants and perturbation parameters within the final deperturbation analysis (for details see text).
[c] Numbers in parentheses are the random (fitting) uncertainties in units of last-significant digit.

Table 11
Term values (in cm^{-1}) of the $A^1\Pi(v = 1)$ level and its perturbers as well as $I^1\Sigma^-(v = 2)$ in $^{13}C^{18}O$.[a,b,c,d]

J	$A^1\Pi(v = 1)$				$e^3\Sigma^-(v = 3)$				$I^1\Sigma^-(v = 2)$	
	F_{1e} (cm^{-1})	$^1\Pi$ (%)	F_{1f} (cm^{-1})	$^1\Pi$ (%)	F_{1e} (cm^{-1})	$^1\Pi$ (%)	F_{2f} (cm^{-1})	$^1\Pi$ (%)	F_{1f} (cm^{-1})	$^1\Pi$ (%)
1	66,178.940(8)	99.64	66,178.938(9)	99.64						
2	66,184.684(6)	99.64	66,184.684(6)	99.64						
3	66,193.301(5)	99.65	66,193.303(6)	99.65					66,609.1(2)	
4	66,204.793(5)	99.66	66,204.793(6)	99.66					66,618.01(6)	
5	66,219.153(5)	99.67	66,219.152(6)	99.67					66,629.14(4)	
6	66,236.387(4)	99.68	66,236.389(6)	99.68					66,642.52(3)	
7	66,256.491(4)	99.69	66,256.493(5)	99.69					66,658.12(3)	
8	66,279.465(4)	99.71	66,279.466(6)	99.70					66,675.95(3)	
9	66,305.307(4)	99.72	66,305.309(5)	99.72					66,696.00(2)	
10	66,334.017(4)	99.74	66,334.019(5)	99.73					66,718.27(2)	
11	66,365.594(4)	99.75	66,365.595(5)	99.75					66,742.76(2)	
12	66,400.035(4)	99.76	66,400.038(5)	99.76					66,769.48(2)	
13	66,437.339(4)	99.78	66,437.341(5)	99.77					66,798.42(2)	
14	66,477.505(4)	99.79	66,477.507(5)	99.79					66,829.57(2)	
15	66,520.532(4)	99.80	66,520.531(5)	99.80					66,862.95(2)	
16	66,566.415(4)	99.81	66,566.414(5)	99.81					66,898.52(2)	
17	66,615.152(4)	99.82	66,615.152(5)	99.82					66,936.32(2)	
18	66,666.742(4)	99.83	66,666.741(5)	99.82					66,976.32(2)	
19	66,721.182(4)	99.84	66,721.179(5)	99.83					67,018.54(2)	
20	66,778.469(4)	99.84	66,778.465(6)	99.83					67,062.96(2)	
21	66,838.598(4)	99.85	66,838.594(6)	99.84					67,109.58(3)	
22	66,901.569(4)	99.85	66,901.562(6)	99.84					67,158.41(3)	
23	66,967.377(4)	99.84	66,967.367(6)	99.83					67,209.44(3)	
24	67,036.015(4)	99.83	67,036.002(6)	99.82						
25	67,107.481(4)	99.80	67,107.463(6)	99.78						
26	67,181.766(4)	99.73	67,181.740(6)	99.70						
27	67,258.840(4)	99.44	67,258.810(6)	99.40						
28	67,338.545(5)	96.36	67,338.502(6)	96.23						
29	67,422.095(5)	95.34	67,422.041(6)	95.33						
30	67,507.387(5)	99.36	67,507.321(7)	99.27						
31	67,595.711(5)	99.69	67,595.615(6)	99.57						

Table 11 (*continued*)

J	$A^1\Pi(v=1)$				$e^3\Sigma^-(v=3)$				$I^1\Sigma^-(v=2)$	
	F_{1e} (cm^{-1})	$^1\Pi$ (%)	F_{1f} (cm^{-1})	$^1\Pi$ (%)	F_{1e} (cm^{-1})	$^1\Pi$ (%)	F_{2f} (cm^{-1})	$^1\Pi$ (%)	F_{1f} (cm^{-1})	$^1\Pi$ (%)
32	67,686.863(6)	99.78	67,686.727(7)	99.58					67,767.56(2)	0.20
33	67,780.819(5)	99.81	67,780.616(6)	99.41						
34	67,877.576(7)	99.82	67,877.211(7)	98.75						
35	67,977.116(7)	99.82	67,976.103(9)	93.09					67,991.37(6)	6.61
36	68,079.429(7)	99.81	68,080.898(9)	88.29					68,068.49(6)	11.23
37	68,184.523(9)	99.78	68,185.048(7)	98.33						
38	68,292.362(9)	99.71	68,292.706(8)	99.22						
39	68,402.946(9)	99.44	68,403.21(2)	99.37			68,534.14(2)	0.06		
40	68,516.16(2)	97.85	68,516.58(2)	99.43						
41	68,632.94(2)	96.33	68,632.60(3)	99.38						
42	68,751.43(3)	99.16	68,751.32(4)	99.00						
43	68,872.79(4)	98.69	68,872.52(3)	97.06	68,802.22(2)	0.12				
44	–	80.62	–	53.53						
45	69,124.62(6)	97.26	69,125.18(4)	96.41			69,090.52(2)	0.78		
	$D^1\Delta(v=1)$				$d^3\Delta(v=6)$					
	F_{1e} (cm^{-1})	$^1\Pi$ (%)	F_{1f} (cm^{-1})	$^1\Pi$ (%)	F_{1e} (cm^{-1})	$^1\Pi$ (%)	F_{2e} (cm^{-1})	$^1\Pi$ (%)	F_{2f} (cm^{-1})	$^1\Pi$ (%)
27			67,286.55(6)	0.44						
28	67,349.06(6)	3.44	67,348.15(2)	3.43						
29	67,412.60(3)	4.53	67,412.56(6)	4.48						
30	67,479.47(3)	0.53	67,479.48(4)	0.53						
31	67,548.31(6)	0.20								
32	67,619.23(6)	0.10								
33										
...										
43									69,009.53(2)	0.31
...										
45					69,097.74(3)	1.68				
46									69,299.05(5)	0.02
47							69,402.51(2)	0.56		
48									69,499.71(5)	2.73

[a] All term values are given in relation to $X^1\Sigma^+(v=0)$ level.
b The terms were merged on the basis of the $^{13}C^{18}O$ $A^1\Pi - X^1\Sigma^+(1,0)$, $B^1\Sigma^+ - A^1\Pi(0,1)$, $C^1\Sigma^+ - A^1\Pi(0,1)$ bands and $C^1\Sigma^+(v=0)$ terms obtained in this work as well as $^{13}C^{18}O$ $B^1\Sigma^+(v=0)$ terms given in Ref. [17] and $X^1\Sigma^+(v=0)$ terms calculated on the basis of Ref. [56].
[c] Numbers in parentheses are the random (fitting) uncertainties in units of last-significant digit.
[d] "$^1\Pi$ (%)" denotes percentage character of the $^{13}C^{18}O$ $A^1\Pi(v=1)$ level.

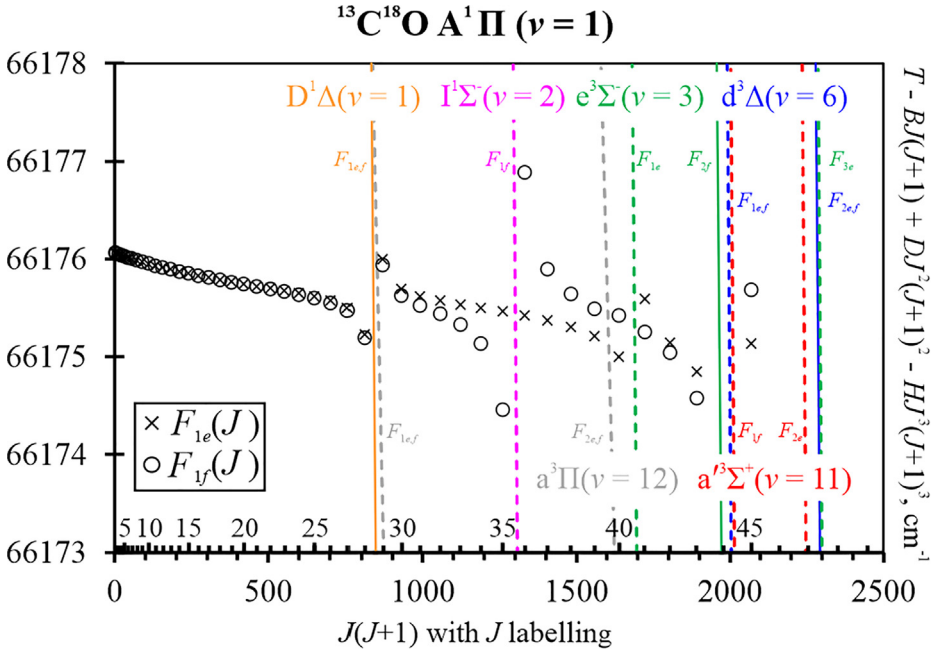

Fig. 5. Reduced ro-vibronic terms of the $A^1\Pi(v=1)$ level and its perturbers in the $^{13}C^{18}O$ isotopologue. Solid lines represent terms, which were calculated based on the experimental extra-line frequencies, whereas dotted lines correspond to the theoretical values. The *T*, *B*, *D*, and *H* values of $A^1\Pi(v=1)$ were taken after deperturbation (see Table 7).

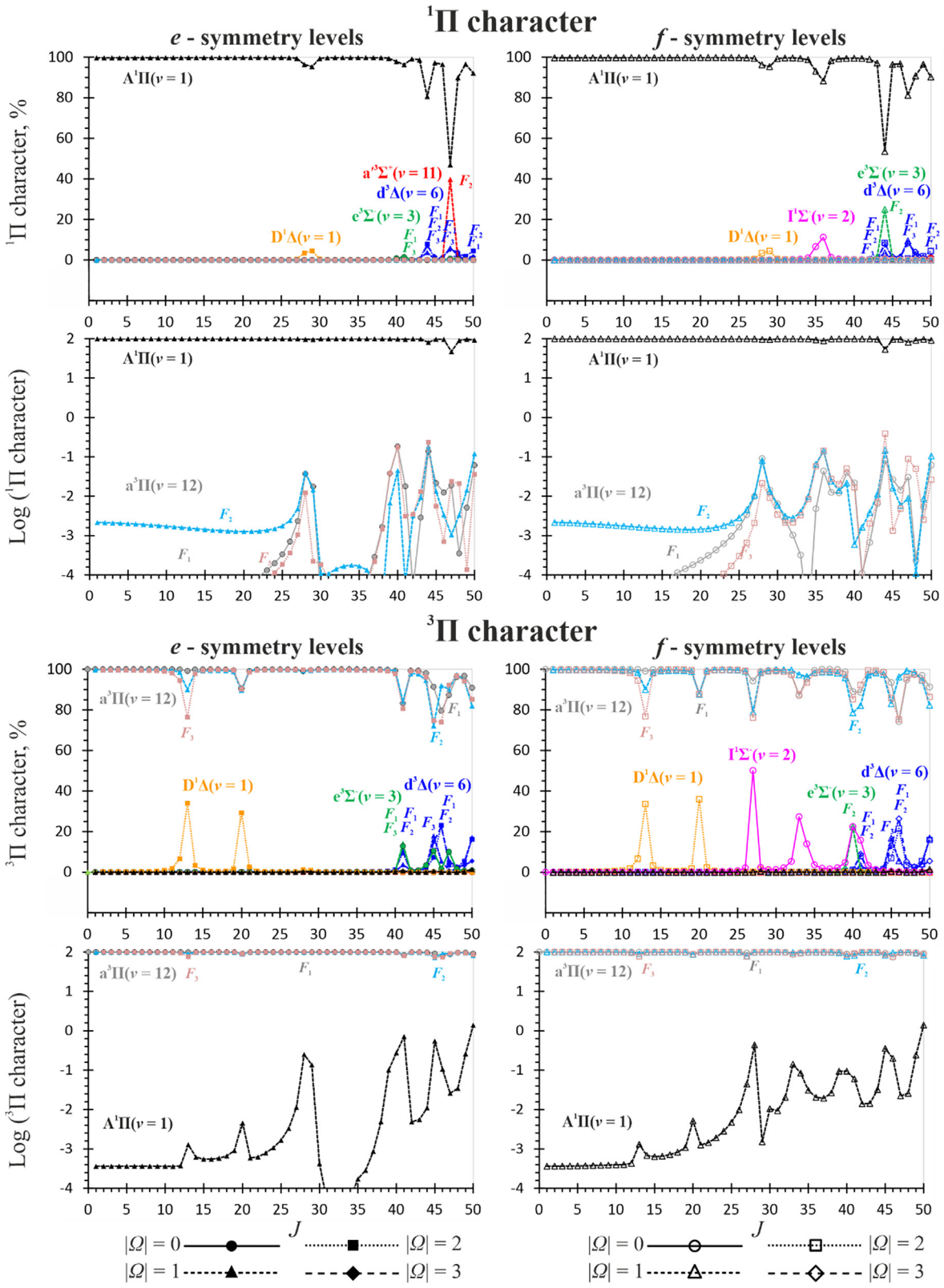

Fig. 6. Percentage $^{1}\Pi$ and $^{3}\Pi$ characters of the states involved in the interactions with the $A^{1}\Pi(v = 1)$ and $a^{3}\Pi(v = 12)$ levels of $^{13}C^{18}O$ (only percentages above 1% are represented by the symbols of the ro-vibrational levels). Detailed amounts of the $^{1}\Pi$ character of the experimental terms are listed in Table 10. The indirect $A^{1}\Pi \sim a^{3}\Pi$ perturbations arising through the $e^{3}\Sigma^{-}(v = 2, 3)$, $d^{3}\Delta(v = 5, 6)$, $D^{1}\Delta(v = 1)$ and $I^{1}\Sigma^{-}(v = 2)$ intermediate states are presented in the lower graphs of each section (see Table 8 for details). Note that the spin states are differentiated by colour only for the $a^{3}\Pi(v = 12)$ level.

model, these levels mixed most at (see Figs. 4 – 6): *(i)* J = 28 with 0.1–0.02% $^1\Pi$-character shared with the a(12) F_{1f} and F_{1e} ($|\Omega|$ = 0) levels, 0.09–0.05% with the F_{2f} and F_{2e} ($|\Omega|$ = 1) levels, 0.03–0.02% with the F_{3f} and F_{3e} ($|\Omega|$ = 2) levels, as a result of the indirect spin–orbit and $\boldsymbol{L}$-uncoupling a(v = 12) ~ D(v = 1, $|\Omega|$ = 2) ~ A (v = 1, $|\Omega|$ = 1) interactions; *(ii)* J = 36 with ~ 0.4% mainly for F_{2f} ($|\Omega|$ = 1) and F_{3f} ($|\Omega|$ = 2), as a result of the indirect spin–orbit and $\boldsymbol{L}$-uncoupling a(v = 12) ~ I(v = 2, $|\Omega|$ = 0) ~ A(v = 1, $|\Omega|$ = 1) interactions; *(iii)* J = 40 with ~ 0.2% mainly for F_{3e} ($|\Omega|$ = 2) and F_{1e} ($|\Omega|$ = 0) as a result of the indirect spin–orbit/spin-electronic/$\boldsymbol{L}$–uncoupling and spin–orbit a(v = 12) ~ e(v = 3, $|\Omega|$ = 0, 1) ~ A (v = 1, $|\Omega|$ = 1) interactions; *(iv)* J = 44 with ~ 0.4%, mainly for F_{3f} ($|\Omega|$ = 2), as a result of the indirect spin–orbit/spin–electronic/$\boldsymbol{L}$–uncoupling and spin–orbit a(v = 12) ~ d(v = 6, $|\Omega|$ = 1) ~ A(v = 1, $|\Omega|$ = 1) interaction.

A new deperturbation extends analysis of the $A^1\Pi(v=1)$ state in the $^{13}C^{18}O$ isotopologue beyond previous work [27,34,58] and was based on a broad set of experimental data from the Fourier-transform spectroscopy of UV synchrotron-absorption and VIS emission in an electric discharge. The final model includes 18 additional intra-molecular interactions, which have not been taken into account previously [27]. The new results extend our knowledge of the energy structure of the $A^1\Pi(v=1)$, $B^1\Sigma^+(v=0)$ and $C^1\Sigma^+(v=0)$ levels of $^{13}C^{18}O$ which are previously unknown for rotational excitation above up J = 30 for $A^1\Pi(v=1)$ [34], J = 31 for $B^1\Sigma^+(v=0)$ [58], and J = 44 for $C^1\Sigma^+(v=0)$ [58]. In this work, it was possible to determine the $A^1\Pi(v=1)$, $B^1\Sigma^+(v=0)$, $C^1\Sigma^+(v=0)$ term values up to J = 45, 50, 60, respectively (see Table 10 and Table 11 for details). These results will contribute in future to the calculation of isotopologue-independent spin–orbit and rotation-electronic perturbation parameters and a mass-reduced all isotopologue fit.

CRediT authorship contribution statement

Stanisław Ryzner: Methodology, Investigation, Formal analysis, Data curation, Validation, Software, Writing – original draft, Writing – review & editing, Visualization. **Marzena I. Malicka:** Visualization, Software, Formal analysis, Data curation. **Alan N. Heays:** Conceptualization, Methodology, Investigation, Writing – original draft, Writing – review & editing, Methodology, Software, Validation, Data curation, Formal analysis, Visualization, Funding acquisition. **Robert W. Field:** Conceptualization, Methodology, Validation, Resources, Writing – review & editing, Funding acquisition. **Nelson de Oliveira:** Investigation, Writing – review & editing. **Wojciech Szajna:** Validation, Writing – review & editing. **Wim Ubachs:** Conceptualization, Investigation, Methodology, Validation, Writing – review & editing, Resources, Funding acquisition. **Rafał Hakalla:** Conceptualization, Supervision, Funding acquisition, Project administration, Methodology, Software, Investigation, Formal analysis, Validation, Resources, Writing – original draft, Writing – review & editing.

Declaration of Competing Interest

The authors declare that they have no known competing financial interests or personal relationships that could have appeared to influence the work reported in this paper.

Acknowledgements

We dedicate this work to the memory of Professor Colin M. Western (University of Bristol), expert in high-resolution molecular spectroscopy, for his outstanding service to the international spectroscopic community in making available the PGOPHER program for analysing spectra in terms of effective Hamiltonians.

RH thanks LASERLAB-EUROPE for support of this research [grants: EUH2020-RIP-654148 and EC's-SPF-284464]. SR, RH and WSz are gratitude to the European Regional Development Fund and the Polish state budget within the framework of the Carpathian Regional Operational Programme [grant number RPPK.01.03.00-18-001/10] for funding the Centre for Innovation and Transfer of Natural Sciences and Engineering Knowledge of the University of Rzeszów. AH acknowledges support by grants no. 19-03314S of the Czech Science Foundation and ERDF/ESF "Centre of Advanced Applied Sciences" (No. CZ.02.1.01/0.0/0.0/16_019/0000778). RWF thanks the US National Science Foundation (grant number CHE-1800410) for support of his research, which includes substantial collaborations. The authors are grateful to the general and technical staff of SOLEIL synchrotron for their support under project numbers 20120653 and 20160118.

Appendix A. Supplementary material

Supplementary data to this article can be found online at https://doi.org/10.1016/j.saa.2022.121367.

References

[1] S.R. Federman, A.E. Glassgold, E.B. Jen7kins, E.J. Shaya, The abundance of CO in diffuse interstellar clouds - an ultraviolet survey, Astrophys J. 242 (1980) 545–559, https://doi.org/10.1086/158489.
[2] W. Langer, A. Penzias, C-12/C-13 isotope ratio in the local interstelar-medium from observations of (CO)-C-13-O-18 in molecular clouds, Astrophys. J. 408 (1993) 539–547, https://doi.org/10.1086/172611.
[3] F. Bensch, I. Pak, J. Wouterloot, G. Klapper, G. Winnewisser, Measurement of rare CO isotopomers toward the rho Ophiuchi molecular cloud, Chem. Diagn. STAR Form. (2003) 254–256.
[4] D.C. Catling, 10.13 - Planetary Atmospheres, in: G. Schubert (Ed.), Treatise Geophys. Second Ed., Elsevier, Oxford, 2015: pp. 429–472. https://doi.org/10.1016/B978-0-444-53802-4.00185-8.
[5] R. Visser, E.F. van Dishoeck, J.H. Black, The photodissociation and chemistry of CO isotopologues: applications to interstellar clouds and circumstellar disks, Astron. Astrophys. 503 (2) (2009) 323–343, https://doi.org/10.1051/0004-6361/200912129.
[6] T.S. Barman, Q.M. Konopacky, B. Macintosh, C. Marois, Simultaneous detection of water, methane, and carbon monoxide in the atmosphere of exoplanet HR 8799 b, Astrophys. J. 804 (2015) 61, https://doi.org/10.1088/0004-637x/804/1/61.
[7] K. Heng, J.R. Lyons, Carbon dioxide in exoplanetary atmospheres: rarely dominant compared to carbon monoxide and water in hot, hydrogen-dominated atmospheres, Astrophys. J. 817 (2016) 149, https://doi.org/10.3847/0004-637x/817/2/149.
[8] M. McJunkin, K. France, E.B. Burgh, G.J. Herczeg, R.N. Schindhelm, J.M. Brown, A. Brown, Probing the inner regions of protoplanetary disks with CO absorption line spectroscopy, Astrophys. J. 766 (1) (2013) 12, https://doi.org/10.1088/0004-637X/766/1/12.
[9] S. Perez, S. Casassus, F. Ménard, P. Roman, G. Van Der Plas, L. Cieza, C. Pinte, V. Christiaens, A.S. Hales, CO gas inside the protoplanetary disk cavity in HD 142527: Disk structure from ALMA, Astrophys J. 798 (2015) 85–97, https://doi.org/10.1088/0004-637X/798/2/85.
[10] K. Zhang, K.R. Schwarz, E.A. Bergin, Rapid Evolution of Volatile CO from the Protostellar Disk Stage to the Protoplanetary Disk Stage, Astrophys. J. Lett. 891 (2020) L17, https://doi.org/10.3847/2041-8213/ab7823.
[11] N. Kameswara Rao, O. De Marco, S. Krishna, J. Murthy, A. Ray, F. Sutaria, R. Mohan, Planetary nebulae with UVIT, A&A. 620 (2018) A138, https://doi.org/10.1051/0004-6361/201833507.
[12] J. Bally, W.D. Langer, Isotope-selective photodestruction of carbon monoxide, Astrophys. J. 255 (1982) 143–148, https://doi.org/10.1086/159812.
[13] C.J. Bennett, C.S. Jamieson, R.I. Kaiser, Mechanistical studies on the formation and destruction of carbon monoxide (CO), carbon dioxide (CO_2), and carbon trioxide (CO_3) in interstellar ice analog samples, Phys. Chem. Chem. Phys. 12 (2010) 4032–4050, https://doi.org/10.1039/B917162B.
[14] A.E. Glassgold, P.J. Huggins, W.D. Langer, Shielding of CO from dissociating radiation in interstellar clouds, Astrophys. J. 290 (1985) 615–626, https://doi.org/10.1086/163019.
[15] M.A.K. Khalil, Decline in atmospheric carbon monoxide raises questions about its cause, Eos Trans. Am. Geophys. Union. 76 (1995) 353–354. https://doi.org/10.1029/95EO00218.
[16] H. Lefebvre-Brion, R.W. Field, The spectra and dynamics of diatomic molecules, in: The Spectra and Dynamics of Diatomic Molecules, Elsevier, 2004, pp. 621–739, https://doi.org/10.1016/B978-012441455-6/50012-3.

[17] R. Hakalla, T.M. Trivikram, A.N. Heays, E.J. Salumbides, N. de Oliveira, R.W. Field, W. Ubachs, Precision spectroscopy and comprehensive analysis of perturbations in the $A^1\Pi(v = 0)$ state of $^{13}C^{18}O$, Mol. Phys. 117 (2019) 79–96, https://doi.org/10.1080/00268976.2018.1495848.

[18] R.W. Field, Spectroscopy and Perturbation Analysis in Excited States of CO and CS, Harvard University, 1971, PhD Thesis.

[19] R.W. Field, B.G. Wicke, J.D. Simmons, S.G. Tilford, Analysis of perturbations in the $a^3\Pi$ and $A^1\Pi$ states of CO, J Mol Spectr. 44 (1972) 383–399, https://doi.org/10.1016/0022-2852(72)90111-7.

[20] M.L. Niu, E.J. Salumbides, D. Zhao, N. de Oliveira, D. Joyeux, L. Nahon, R.W. Field, W. Ubachs, High resolution spectroscopy and perturbation analysis of the CO $A^1\Pi$ - $X^1\Sigma^+$ (0,0) and (1,0) bands, Mol Phys. 111 (14-15) (2013) 2163–2174, https://doi.org/10.1080/00268976.2013.793889.

[21] M.L. Niu, E.J. Salumbides, A.N. Heays, N. de Oliveira, R.W. Field, W. Ubachs, Spectroscopy and perturbation analysis of the CO $A^1\Pi$-$X^1\Sigma^+$(2,0), (3,0) and (4,0) bands, Mol Phys. 114 (5) (2016) 627–636, https://doi.org/10.1080/00268976.2015.1108472.

[22] M.L. Niu, R. Hakalla, T.M. Trivikram, A.N. Heays, N. de Oliveira, E.J. Salumbides, W. Ubachs, Spectroscopy and perturbation analysis of the $A^1\Pi(v{=}0)$ state of $^{13}C^{16}O$, Mol Phys. 114 (19) (2016) 2857–2867, https://doi.org/10.1080/00268976.2016.1218078.

[23] T.M. Trivikram, R. Hakalla, A.N. Heays, M.L. Niu, S. Scheidegger, E.J. Salumbides, N. de Oliveira, R.W. Field, W. Ubachs, Perturbations in the $A^1\Pi$, $v = 0$ state of $^{12}C^{18}O$ investigated via complementary spectroscopic techniques, Mol Phys. 115 (24) (2017) 3178–3191, https://doi.org/10.1080/00268976.2017.1356477.

[24] R. Hakalla, M.L. Niu, R.W. Field, E.J. Salumbides, A.N. Heays, G. Stark, J.R. Lyons, M. Eidelsberg, J.L. Lemaire, S.R. Federman, M. Zachwieja, W. Szajna, P. Kolek, I. Piotrowska, M. Ostrowska-Kopeć, R. Kępa, N. de Oliveira, W. Ubachs, VIS and VUV spectroscopy of $^{12}C^{17}O$ and deperturbation analysis of the $A^1\Pi$, $v = 1$–5 levels, Roy Soc Chem Adv. 6 (2016) 31588–31606, https://doi.org/10.1039/c6ra01358a.

[25] R. Hakalla, M.L. Niu, R.W. Field, A.N. Heays, E.J. Salumbides, G. Stark, J.R. Lyons, M. Eidelsberg, J.L. Lemaire, S.R. Federman, N. de Oliveira, W. Ubachs, Fourier-transform spectroscopy of $^{13}C^{17}O$ and deperturbation analysis of the $A^1\Pi(v = 0$–$3)$ levels, J. Quant. Spectrosc. Radiat. Transf. 189 (2017) 312–328, https://doi.org/10.1016/j.jqsrt.2016.12.012.

[26] M.I. Malicka, S. Ryzner, A.N. Heays, N. de Oliveira, R.W. Field, W. Ubachs, R. Hakalla, High-resolution Fourier-transform spectroscopy and deperturbation analysis of the $A^1\Pi(v = 1)$ level in $^{12}C^{18}O$, J. Quant. Spectrosc. Radiat. Transf. 255 (2020), https://doi.org/10.1016/j.jqsrt.2020.107243 107243.

[27] C. Haridass, S.P. Reddy, A.C. Lefloch, The fourth positive ($A^1\Pi$ – $X^1\Sigma^+$) system of $^{12}C^{18}O$ and $^{13}C^{18}O$: Perturbations in the $A^1\Pi$ state, J. Mol. Spectrosc. 167 (2) (1994) 334–352, https://doi.org/10.1006/jmsp.1994.1240.

[28] W. Ubachs, K.S.E. Eikema, W. Hogervorst, P.C. Cacciani, Narrow-band tunable extreme-ultraviolet laser source for lifetime measurements and precision spectroscopy, J Opt Soc Am B. 14 (1997) 2469–2476, https://doi.org/10.1364/JOSAB.14.002469.

[29] Z. Malak, M. Rytel, J.D. Janjić, D.S. Pešić, Ångström system of the $^{13}C^{18}O$ molecule, Acta Phys Hung. 55 (1984) 85–95, https://doi.org/10.1007/BF03155922.

[30] C.V.V. Prasad, G.L. Bhale, S.P. Reddy, The Ångström ($B^1\Sigma^+$ – $A^1\Pi$) band system of $^{13}C^{18}O$, J Mol Spectr. 104 (1) (1984) 165–173, https://doi.org/10.1016/0022-2852(84)90252-2.

[31] C.V.V. Prasad, S.P. Reddy, M. Sandys-Wunsch, The Herzberg ($C^1\Sigma^+$ – $A^1\Pi$) band system of $^{13}C^{18}O$, J. Mol. Spectrosc. 114 (2) (1985) 436–444, https://doi.org/10.1016/0022-2852(85)90236-X.

[32] R. Kępa, High-resolution studies of the Herzberg band system ($C^1\Sigma^+$ – $A^1\Pi$) in the $^{13}C^{18}O$ molecule, Can J Phys. 66 (11) (1988) 1012–1024, https://doi.org/10.1139/p88-163.

[33] R. Kepa, The 0–1 and 0–2 Bands of the $E^1\Pi$ – $A^1\Pi$ System of the $^{13}C^{18}O$ Molecule, J. Mol. Spectrosc. 132 (2) (1988) 545–549, https://doi.org/10.1016/0022-2852(88)90344-X.

[34] J.L. Lemaire, M. Eidelsberg, A.N. Heays, L. Gavilan, S.R. Federman, G. Stark, J.R. Lyons, N. de Oliveira, D. Joyeux, High-resolution spectroscopy of the $A^1\Pi(v{=}0$–$10)$ – $X^1\Sigma^+(v{=}0)$ bands in $^{13}C^{18}O$: term values, ro-vibrational oscillator strengths and Höhnl-London corrections, J Phys B. 49 (2016), https://doi.org/10.1088/0953-4075/49/15/154001 154001.

[35] M.I. Malicka, S. Ryzner, A.N. Heays, N. de Oliveira, R.W. Field, W. Ubachs, R. Hakalla, Deperturbation analysis of the $A^1\Pi(v = 2)$ level in the $^{12}C^{18}O$ isotopologue, J. Quant. Spectrosc. Radiat. Transf. 273 (2021), https://doi.org/10.1016/j.jqsrt.2021.107837 107837.

[36] R. Hakalla, M. Zachwieja, W. Szajna, First Analysis of the 1–v″ Progression of the Ångström ($B^1\Sigma^+$–$A^1\Pi$) Band System in the Rare $^{13}C^{17}O$ Isotopologue, J. Phys. Chem. A. 117 (47) (2013) 12299–12312, https://doi.org/10.1021/jp4077239.

[37] R. Hakalla, W. Szajna, M. Zachwieja, Extended analysis of the Ångström band system ($B^1\Sigma^+$–$A^1\Pi$) in the rare $^{12}C^{17}O$ isotopologue, J. Phys. B At. Mol. Opt. Phys. 45 (21) (2012) 215102, https://doi.org/10.1088/0953-4075/45/21/215102.

[38] R. Hakalla, W. Szajna, M. Zachwieja, R. Kępa, Reanalysis of the Ångström System ($B^1\Sigma^+$- $A^1\Pi$) in the $^{13}C^{16}O$ Isotopic Molecule, Acta Phys. Pol. A. 122 (2012) 674–682, https://doi.org/10.12693/APhysPolA.122.674.

[39] R. Hakalla, M. Zachwieja, W. Szajna, First Analysis of the B1Σ+(v=1) Rydberg state in the lesser-abundant 12C17O isotopologue on the basis of the 1–v'' progression of the Ångström band system, J Quant Spectr Rad Transf. 140 (2014) 7–17, https://doi.org/10.1016/j.jqsrt.2014.02.004.

[40] Bruker, OPUS: spectroscopy software for state-of-the-art measurement, processing and evaluation of IR, NIR and Raman Spectra. v.8.5.29., Bruker Optik GmbH, 2019.

[41] J.W. Brault, High precision Fourier-transform spectrometry: The critical role of phase corrections, Microchim. Acta. 93 (1-6) (1987) 215–227, https://doi.org/10.1007/BF01201691.

[42] C.M. Western, PGOPHER: A program for simulating rotational, vibrational and electronic spectra, J Quant Spectr Rad Transf. 186 (2017) 221–242, https://doi.org/10.1016/j.jqsrt.2016.04.010.

[43] C.M. Western, PGOPHER: A program for simulating rotational structure. Development version. 11.0.136. University of Bristol, Bristol., (2020). http://pgopher.chm.bris.ac.uk.

[44] J.D. Janjić, L.U. Čonkić, D.S. Pešić, R. Kepa, M. Rytel, The Herzberg system of $^{12}C^{18}O$ molecule, J Mol Spectr. 72 (2) (1978) 297–300, https://doi.org/10.1016/0022-2852(78)90130-3.

[45] N. de Oliveira, D. Joyeux, D. Phalippou, J.C. Rodier, F. Polack, M. Vervloet, L. Nahon, A Fourier transform spectrometer without a beam splitter for the vacuum ultraviolet range: From the optical design to the first UV spectrum, Rev Sci. Instr. 80 (4) (2009) 043101, https://doi.org/10.1063/1.3111452.

[46] L. Nahon, N. de Oliveira, G.A. Garcia, J.-F. Gil, B. Pilette, O. Marcouillé, B. Lagarde, F. Polack, DESIRS: a state-of-the-art VUV beamline featuring high resolution and variable polarization for spectroscopy and dichroism at SOLEIL, J. Synchrotron Radiat. 19 (4) (2012) 508–520, https://doi.org/10.1107/S0909049512010588.

[47] A.C. Le Floch, F. Launay, J. Rostas, R.W. Field, C.M. Brown, K. Yoshino, Reinvestigation of the CO $A^1\Pi$ state and its perturbations: The $v = 0$ level, J Mol Spectr. 121 (2) (1987) 337–379, https://doi.org/10.1016/0022-2852(87)90056-7.

[48] A. Le Floch, J. Rostas, J. Schamps, The $A^1\Pi \sim {}^D1\Delta$ rotation-electronic interaction in CO, Mol. Phys. 63 (4) (1988) 677–684, https://doi.org/10.1080/00268978800100481.

[49] N. Åslund, Numerical-method for simultaneous determination of term values and molecular-constants, J Mol Spectr. (1974) 424–434, https://doi.org/10.1016/0022-2852(74)90245-8.

[50] R.F. Curl, C.B. Dane, Unbiased least-squares fitting of lower states, J Mol Spectr. 128 (2) (1988) 406–412, https://doi.org/10.1016/0022-2852(88)90157-9.

[51] J. Watson, On the use of term values in the least-squares fitting spectra, J Mol Spectr. (1989) 302–308, https://doi.org/10.1016/0022-2852(89)90119-7.

[52] C. Focsa, A. Poclet, B. Pinchemel, R. Le Roy, P. Bernath, Fourier transform spectroscopy of the $A'^1\Pi$-$X^1\Sigma^+$ system of CaO, J. Mol. Spectrosc. 203 (2000) 330–338, https://doi.org/10.1006/jmsp.2000.8187.

[53] R. Hakalla, W. Szajna, I. Piotrowska, M.I. Malicka, M. Zachwieja, R. Kępa, Fourier-transform spectroscopy of the $A^2\Pi_i$ – $X^2\Sigma^+$ system in CO^+ and deperturbation analysis of the $A^2\Pi_i(v = 0, 1)$ levels, J. Quant. Spectrosc. Radiat. Transf. 234 (2019) 159–176, https://doi.org/10.1016/j.jqsrt.2019.05.030.

[54] C. Kittrell, B.A. Garetz, Analysis of the $D^1\Delta$ – $X^1\Sigma^+$ transition in CO observed by two-photon excitation, Spectrochim Acta. 1 (1989) 31–40. https://doi.org/0.1016/0584-8539(89)80024-8.

[55] S. Yamamoto, S. Saito, The microwave spectra of CO in the electronically excited states $a^3\Pi$ and $a'^3\Sigma^+$, J Chem Phys. 89 (1988) 1936–1944, https://doi.org/10.1063/1.455091.

[56] J.A. Coxon, P.G. Hajigeorgiou, Direct potential fit analysis of the $X^1\Sigma^+$ ground state of CO, J Chem Phys. 121 (2004) 2992–3008, https://doi.org/10.1063/1.1768167.

[57] B.A. Garetz, C. Kittrell, A.C. Le Floch, Analysis of the two-photon $D^1\Delta$ – $X^1\Sigma^+$ transition in CO: Perturbations in the (10–0) band, J Chem Phys. 94 (1991) 843–853, https://doi.org/10.1063/1.459973.

[58] J.L. Lemaire, A.N. Heays, M. Eidelsberg, L. Gavilan, G. Stark, S.R. Federman, J.R. Lyons, N. de Oliveira, Atlas of new and revised high-resolution spectroscopy of six CO isotopologues in the 101–115 nm range, A&A. 614 (2018) A114, https://doi.org/10.1051/0004-6361/201732114.

[59] J.K.G. Watson, Rounding errors in the reporting of least-squares parameters, J. Mol. Spectrosc. 66 (3) (1977) 500–502, https://doi.org/10.1016/0022-2852(77)90308-3.

[60] E. Hirota, J. Brown, J. Hougen, T. Shida, N. Hirota, Symbols for fine and hyperfine-structure parameters, Pure Appl. Chem. 66 (1994) 571–576, https://doi.org/10.1351/pac199466030571.

[61] M. Eidelsberg, J.-Y. Roncin, A. Le Floch, F. Launay, C. Letzelter, J. Rostas, Reinvestigation of the vacuum ultraviolet spectrum of CO and isotopic species: The B-X transition, J Mol Spectr. 121 (1987) 309–336, https://doi.org/10.1016/0022-2852(87)90055-5.